ELECTRONIC SUPPLEMENTARY INFORMATION (ESI)

Global climate change and contaminants – an overview of opportunities and priorities for modelling the potential implications for long-term human exposure to organic compounds in the Arctic

James M. Armitage[1,2*], Cristina L. Quinn[2], Frank Wania[2]

1. *Department of Occupational Medicine, Aarhus University Hospital, Noerrebrogade 44, Aarhus C, Denmark 8000*
2. *Department of Physical and Environmental Sciences, University of Toronto Scarborough, 1265 Military Trail, Toronto, Ontario, Canada M1C 1A4*

* Corresponding author. Tel.: +1 416 287 7277; Email address: james.armitage@utoronto.ca

Contents (43 pages, 15 figures, 20 tables)

<u>Section S1</u> Summary of some key global climate change projections presented in ACIA (2005)

The 2005 Arctic Climate Impact Assessment report[1] presents climate change scenarios for the Arctic environment (60 °N and above) based on the IPCC greenhouse gas (GHG) emission scenarios. Depending on the GHG emission scenario, global mean surface air temperatures are projected to increase by 1 to 2 °C by the mid-21st century relative to 1990 whereas an increase of 2 to 4.5 °C is projected for the year 2100. Annual average precipitation in the northern hemisphere is projected to decrease in some regions (e.g. S. Europe and S. USA) but generally increase overall, with the largest percentage increases projected for the Arctic (up to ~ +20% annually by 2100). Baseline temperature and precipitation rates (1981-2000 multi-year average) are summarized in Table S1 whereas some key projections based on ACIA-designated models are presented in Table S2. Potential changes to primary productivity are described below.

Table S1 Global and Arctic climatological baselines (1981 – 2000) presented in ACIA[1]

	Global		Arctic	
	Surface Temperature (air, °C)	Precipitation (mm d^{-1})	Surface Temperature (air, °C)	Precipitation (mm d^{-1})
Winter (Dec–Feb)	12.4	2.70	-21.5	1.12
Spring (Mar–May)	13.8	2.72	-11.6	1.05
Summer (June–Aug)	15.5	2.89	5.7	1.67
Autumn (Sept–Nov)	13.9	2.69	-8.6	1.31
Annual	13.9	2.75 (1005 mm yr^{-1})	-8.8	1.28 (465 mm yr^{-1})

Primary Productivity

The main factors controlling primary productivity (PP) in the Arctic Ocean are light limitation (in areas presently covered by multi-year sea ice) and nutrient limitation (particularly in highly stratified waters). Scenarios for PP described in the ACIA[1] are as follows:

i) Light-limited regions: ↑ 2–5-fold, due to sea-ice disappearance, assuming no nutrient limitation
ii) Barents Sea: ↑ ≥ 2-fold due to deeper wind-mixed layer and supply of nutrients from underlying Atlantic water
iii) Arctic shelf seas: ↑ ≥ 2-fold due to retreat of permanent ice pack beyond shelf break and subsequent onset of enhanced upwelling and exchange with nutrient-rich offshore waters

More recent studies incorporating model simulations suggest far more modest changes. For example, Lavoie et al.[2] employed a coupled sea ice-ocean-biological 1D model to project future PP for the Mackenzie Shelf (Beaufort Sea); projected increases in average annual PP are low (↑ 6 and 9% for 2050 and 2090 respectively vs. present day), primarily due to the influence of enhanced fresh water input (intensified stratification, reduced replenishment of nutrients). Similarly, Ellingsen et al.[3] applied a coupled hydrodynamic-ecological model for the Barents Sea and reported only an 8% increase in PP over the next 65 years.

Table S2 Summary of some key model projections for the global and Arctic environment presented in ACIA[1]. Ranges reflect output from five different models

Parameter	Projected Changes (relative to 1981–2000)	
B2 Scenario (IPCC)		
Mean annual temperature (global) 2071-2090	+1.9 (1.4–2.1) °C	
Mean annual temperature (Arctic) 2011–2030 2041–2060 2071–2090	+1.2 (1.0–1.5) °C +2.5 (2.2–3.2) °C +3.7 (2.8–4.6) °C	
Temperature over central Arctic Summer (2071–2090) Autumn (2071–2090)	~ +0.5–1.0 °C ~ +6.0–10.0 °C	
Mean annual precipitation 2011–2030 2041–2060 2071–2090	+4.3 (2.3–8.3)% +7.9 (4.6–12.3)% +12.3 (7.5–18.1)%; in winter (up to +35%)	
Projections and/or Extrapolations		
Snow cover extent (area) 2011–2030 2041–2060 2071–2090	–4 to –7% –5 to –13% –9 to –17%	
Sea-ice extent (10^6 km^2)	March	September
1981 – 2000	16.14 – 16.32	7.02 – 7.41
2011 – 2030	15.00 – 15.62	3.33 – 7.00
2041 – 2060	13.94 – 14.97	0.55 – 6.72
2071 - 2090	13.26 – 14.52	0.05 – 6.59
Sea-ice cover (duration) 2020 2050 2080	Shorter by 10 days Shorter by 15–20 days Shorter by 20–30 days	
Total Permafrost (% of current surface area) 2030 2050 2080	82–90% 71–87% 65–81%; Depth of seasonal thaw ↑ ≥ 50%	
River discharge (Arctic)	+5–25%	

Section S2 Supporting Information for Figure 2, long-term simulation of PCB-153 in the global environment

Physical-chemical properties used in the simulation are presented in Table S3 and the emission scenario in Figure S1. Modelled air concentrations in the Arctic (N-Polar) and main source region (N-Temperate) over the period 1930–2100 are presented in Figure S2.

Table S3 Partition coefficients and degradation rate constants (or half-lives) selected for this simulation; based on Schenker et al.[4] and Wania & Mackay[5]

Partitioning			
log K_{OW}	7.31	ΔU_{OW}	-26.6 kJ mol^{-1}
log K_{AW}	-2.13	ΔU_{AW}	68.2 kJ mol^{-1}
log K_{OA}	9.45	ΔU_{OW}	-94.8 kJ mol^{-1}
Degradation			
k_{OH}	1.6x10^{-13} cm^3 molecules^{-1} s^{-1}	E_A	10 kJ mol^{-1}
HL$_{Water}$	55000 h	E_A	30 kJ mol^{-1}
HL$_{Sediment}$	170000 h	E_A	30 kJ mol^{-1}
HL$_{Soil}$	550000 h	E_A	30 kJ mol^{-1}

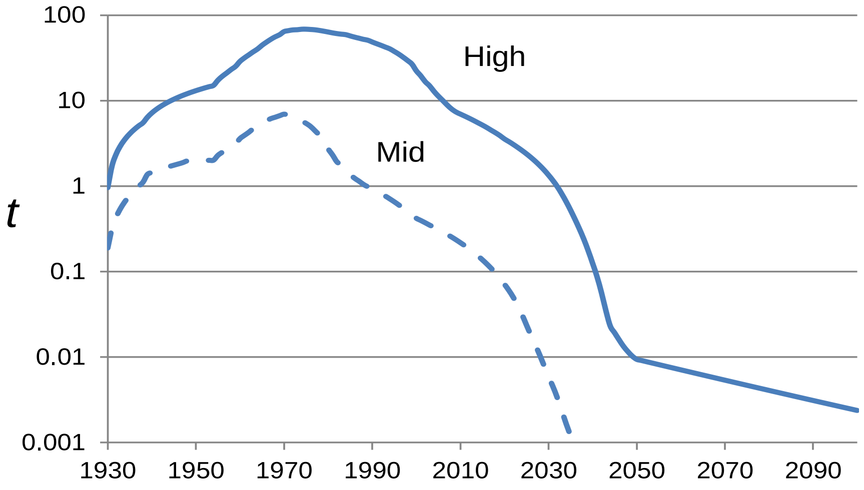

Figure S1 Annual ‘High’ and ‘Mid’ emission estimates[6] for PCB-153 (*t*) over the period 1930–2100

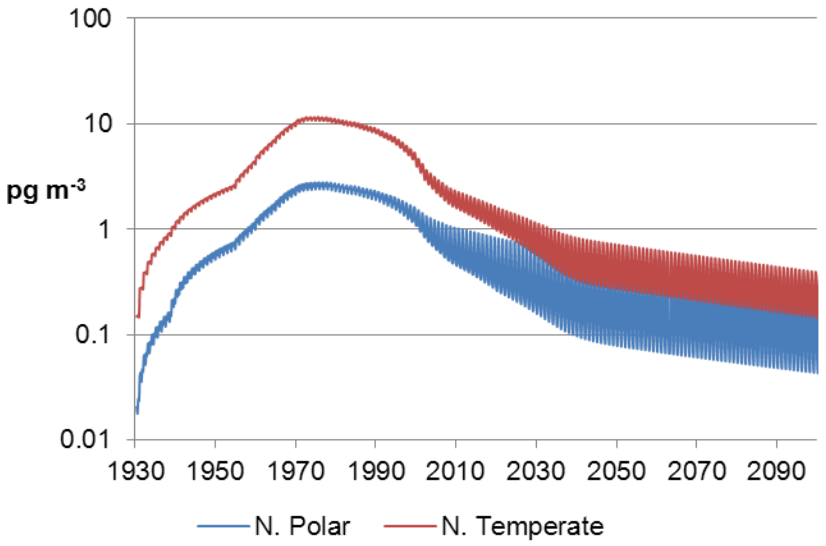

Figure S2 Modelled concentrations in air (total) in main source region (N-Temperate, red) and Arctic environment (N-Polar, blue) over the period 1930 – 2100.

As illustrated in Figure S2, total air concentrations in the main source (N-Temperate) and remote region (N-Polar) essentially follow the pattern in primary emissions over the period 1930 to 2000. Seasonal variability in primary emission levels was deliberately omitted for this simulation although an argument could be made to include this feature in additional simulations based on the nature of PCB emissions (i.e. some portion related to temperature-dependent passive volatilization) and available monitoring data (e.g. see below). Regardless, as primary emissions decline and the importance of secondary sources increases, seasonal variability in total air concentrations becomes very prominent, (and may potentially be a measurable indicator of when dominance of secondary sources prevails). For example, the modelled seasonal pattern in air concentrations varies nearly an order of magnitude in the N-Polar region once secondary sources dominate, with maximum yearly concentrations in summer. The overall trend is still a decline and peak air concentrations (1970s) are not approached.

While a complete model evaluation is beyond the scope of this exercise, some comparisons between available monitoring data and model output for atmosphere and surface ocean are presented here to lend some support to the illustrative results. Comparisons to EMEP monitoring data[7] for air concentrations (total) corresponding to three climatic zones (N-Polar, N-Boreal, N-Temperate) are presented in Figures S3–S5 and a comparison between measured[8] and modelled total water concentrations is presented in Table S4.

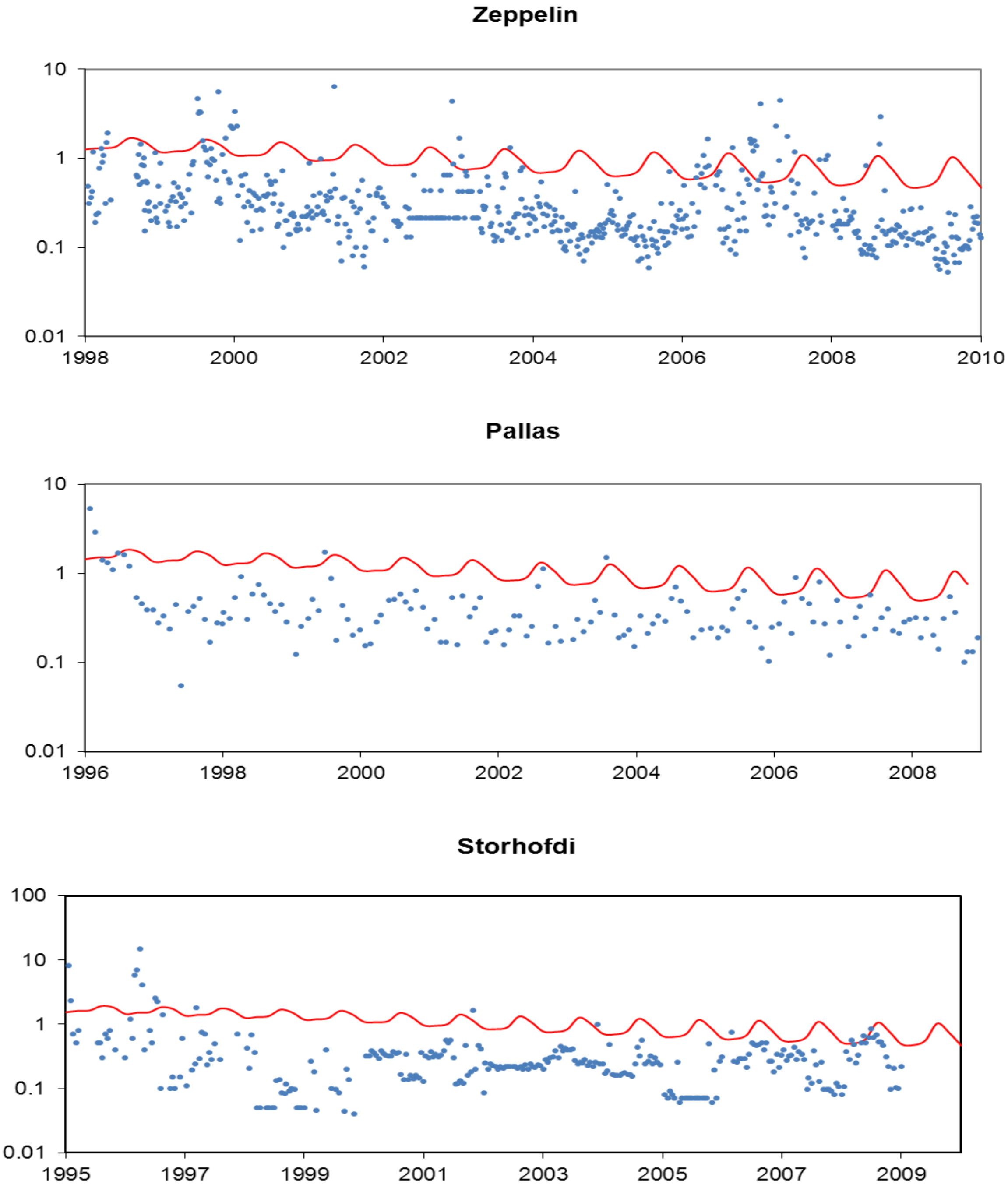

Figure S3 Comparison of PCB-153 total air concentrations (pg m^{-3}) reported at EMEP monitoring stations[7] to model output (red line) for the corresponding climatic zone (N-Polar) of the GloboPOP model.

Modelled air concentrations in the N-Polar region tend to overestimate the reported values at the three monitoring sites but are generally within a factor of ten.

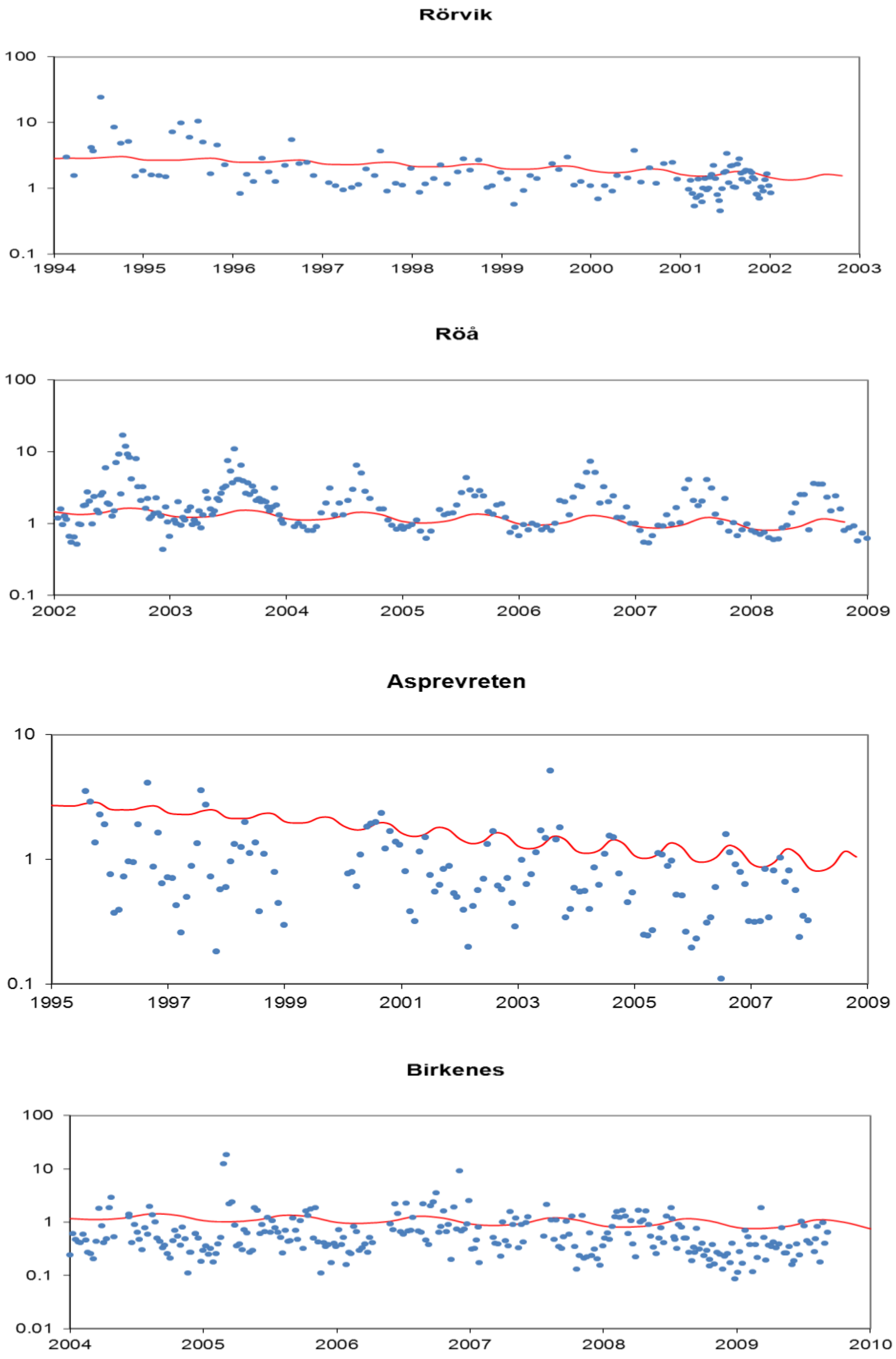

Figure S4 Comparison of PCB-153 total air concentrations (pg m^{-3}) reported at EMEP[7] monitoring stations to model output (red line) for the corresponding climatic zone (N. Boreal) of the GloboPOP model.

Agreement between modeled concentrations and measurements from stations in the N-Boreal region is generally better than for the N-Polar region (i.e. a factor of 5–10 or less) and is not systematically biased towards under- or overestimation.

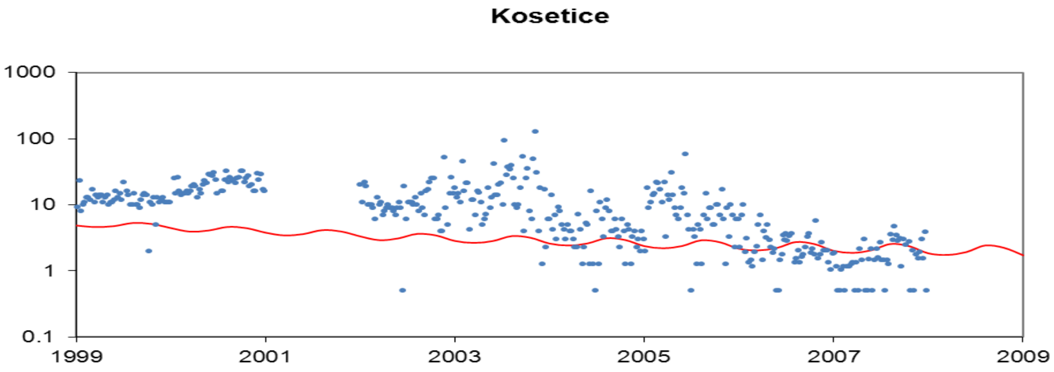

Figure S5 Comparison of PCB-153 total air concentrations (pg m^{-3}) reported at EMEP[7] monitoring stations to model output (red line) for the corresponding climatic zone (N. Temperate) of the GloboPOP model.

Modeled concentrations of PCB-153 tend to underestimate the reported concentrations at the monitoring site in the N. Temperature zone over the period 1999–2005 but are generally within an order of magnitude over the time-series.

Table S4 Comparison of reported total surface ocean water concentrations of PCB-153 in the Arctic[8] with GloboPOP model output

Cruise/Year		Reported Concentrations (total, fg L^{-1})	Model Output for corresponding year (total, fg L^{-1})
AO-01 2001 Expedition	Median (Range)	74 (12–366)	178
Beringia 2005 Expedition	Median (Range)	144 (34–395)	125
ISSS08 2008 Expedition	Median (Range)	154 (67–475)	100

Due to the coarse spatial resolution of the model, the regional differences observed in Carrizo and Gustafsson[8] cannot be represented; the most appropriate comparison is therefore between the central tendency of all monitoring data and model output (which represents an average value). Agreement between measurements and model output on this basis is excellent. The apparent temporal trend in the monitoring data should not be over-interpreted; sampling locations were not consistent between the expeditions and included (depending on the study) sites near estuaries, on the continental shelf and towards the central Arctic.

Section S3 Summary of temporal trends of contaminants in humans inhabiting the Canadian Arctic

Table S5 Summary of temporal trends in blood levels of organic contaminants in pregnant women from different subpopulations in the Canadian Arctic (Donaldson et al.[9])

Region/Subpopulation	**Time Span**	**Compounds**	**Change in levels**[*] (µg L^{-1}/µg kg^{-1} plasma lipids)
Inuvik Dene/Métis	1998/99 vs. 2005/06	THg	1.1 ↓ to 0.7, $p > 0.05$
		PCB-138	10 ↓ to 3.1, $p < 0.001$
		PCB-153	16 ↓ to 5.9, $p < 0.001$
		PCB-180	8.2 ↓ to 3.5, $p < 0.05$
		DDE	64 ↓ to 35, $p < 0.05$
		oxychlordane	4.4 ↓ to 1.6, $p < 0.001$
		t-nonachlor	6.2 ↓ to 2.2, $p < 0.001$
		Toxaphene	1.7 ↓ to 0.5, $p < 0.001$
Inuvialuit	1998/99 vs. 2005/06	THg	2.1 ↓ to 1.1, $p < 0.01$
		PCB-138	22 ↓ to 8.6, $p < 0.001$
		PCB-153	30 ↓ to 17, $p < 0.01$
		PCB-180	9.4 ↓ to 6.8, $p > 0.05$
		DDE	125 ↓ to 76, $p < 0.001$
		oxychlordane	18 ↓ to 8.7, $p < 0.01$
		t-nonachlor	33 ↓ to 14, $p < 0.01$
		Toxaphene	6.8 ↓ to 2.9, $p < 0.01$
Nunavik (N. Québec) Inuit	1992–2007	THg	12 ↓ to 4.0, $p < 0.0001$
		PCB-138	114 ↓ to 22, $p < 0.0001$
		PCB-153	172 ↓ to 40, $p < 0.0001$
		PCB-180	90 ↓ to 16, $p < 0.0001$
		DDE	636 ↓ to 231, $p < 0.0001$
		oxychlordane	77 ↓ to 22, $p < 0.0001$
		t-nonachlor	114 ↓ to 44, $p < 0.0001$

[*] Geometric means: THg reported as µg L^{-1} whole blood, organic contaminants as µg kg^{-1} plasma lipids

There are some caveats related to interpretation of these temporal trends, particularly the 1998/99 vs. 2005/06 comparison. For example, the samples do not necessarily represent a random selection from the population and are limited in number (i.e. small sample size). See Donaldson et al.[9] for more details and discussion of these results.

Section S4 Compilation of partition coefficients and internal energies of phase change for a selection of legacy and current-use chemicals.

Table S6 Key partition coefficients and temperature-dependencies for a selection of widely studied contaminants[4,10-21]

Compound	**log K_{OW}**	**ΔU_{OW} (kJ mol^{-1})**	**log K_{OA}**	**ΔU_{OA} (kJ mol^{-1})**	**log K_{AW}**	**ΔU_{AW} (kJ mol^{-1})**
PCB-28	5.92	-26.6	7.86	-78.4	-1.93	51.8
PCB-52	6.26	-27.5	8.22	-81.3	-1.96	53.8
PCB-101	6.76	-19.3	8.83	-84.4	-2.08	65.2
PCB-118	7.08	-24.5	9.44	-89.8	-2.36	65.2
PCB-138	7.70	-22.2	9.67	-86.9	-1.97	64.7
PCB-153	7.31	-26.6	9.45	-94.8	-2.13	68.2
PCB-180	7.66	-24.7	10.17	-95.2	-2.51	69.0
HCB	5.64	-24.7	7.21	-75.2	-1.58	50.5
p,p'-DDE	6.93	-20.0*	9.70	-98.0	-2.77	78.0
p,p'-DDT	6.39	-20.0*	9.73	-88.1	-3.37	68.1
α-HCH	3.94	-5.10	7.46	-61.9	-3.53	56.8
β-HCH	3.91	-16.2	8.74	-84.1	-4.83	67.8
γ-HCH	3.83	-10.2	7.74	-67.4	-3.91	57.2
PBDE 15	5.48	-20.0*	8.63	-85.2	-2.78	65.2
PBDE 28	5.80	-20.0*	9.41	-90.9	-3.11	70.9
PBDE 47	6.39	-20.0*	10.44	-98.3	-3.35	78.3
PBDE 99	6.76	-20.0*	11.26	-104.2	-3.67	84.2
PBDE 100	6.53	-20.0*	11.02	-107.5	-3.81	87.5
PDBE 153	7.08	-20.0*	11.89	-112.1	-3.86	92.1
Bisphenol A	3.40	-20.0*	12.41	-113.9	-9.01	93.9
DEHP	7.73	-20.0*	10.53	-107.9	-2.80	87.9
DINP	8.60	-20.0*	11.03	-112.9	-2.43	92.9
Alachlor	3.09	-20.0*	9.31	-88.2	-6.22	68.2
Atrazine	2.40	-20.0*	9.08	-85.2	-6.68	65.2
Chlorpyrifos	5.11	-20.0*	8.75	-89.6	-3.64	69.6
Chlorothalonil	3.05	-20.0*	7.14	-94.5	-4.09	74.5
Dacthal	4.24	-20.0*	8.28	-86.7	-4.04	66.7
Diazinon	3.81	-20.0*	8.87	-85.9	-5.06	65.9
Dicofol	5.02	-20.0*	10.03	-100.5	-5.01	80.5
Methoxychlor	5.08	-20.0*	10.16	-101.7	-5.08	81.7
Pentachloroanisole	5.45	-20.0*	7.80	-72.2	-2.35	52.2
Trifluralin	5.34	-20.0*	7.72	-83.5	-2.38	63.5

* assumed default value[22]

In many cases, empirical data on the temperature dependence of these partition coefficients are not available. However, based on Trouton's Rule, Macleod et al.[23] proposed that the internal energy of vaporization (ΔU_A, kJ mol^{-1}) can be estimated from sub-cooled liquid vapour pressure (P_L, Pa) as a first approximation as shown below.

$$\Delta U_A = -3.82 \ln P_L + 67.5$$

Assuming that the temperature dependence of water (ΔU_W) and octanol (ΔU_O) solubility are 0 and 20 kJ mol^{-1} respectively[22], the temperature dependence of partition coefficients can be estimated based on these values and the requirement of thermodynamic consistency i.e.

$$\Delta U_{OW} = \Delta U_O - \Delta U_W$$
$$\Delta U_{OA} = \Delta U_O - \Delta U_A$$
$$\Delta U_{AW} = \Delta U_{OW} - \Delta U_{OA}$$

This estimation approach is most reliable for neutral organic chemicals which are not capable of engaging in hydrogen bonding and/or are not highly polar as such chemicals tend to deviate substantially from Trouton's Rule[23]. Also note that the assumed values of ΔU_W and ΔU_O represent another source of potential error.

Section S5 Illustrative temperature dependence comparisons

Table S7 Factors of change for passive volatilization and abiotic degradation reactions using a range of temperature-dependencies and possible temperature increases assuming a baseline temperature of -5 and 15 °C.

Process		ΔU_A / E_A (kJ mol^{-1})	T_{REF} (°C)	Factor of Change		
				+2 °C	+5 °C	+8 °C
(Re-)Emission	Volatilization	40	-5	1.14	1.39	1.68
			15	1.12	1.33	1.57
		100	-5	1.39	2.27	3.67
			15	1.33	2.04	3.08
Degradation	OH radical reactions (atmosphere)	10	-5	1.03	1.08	1.13
			15	1.03	1.07	1.12
	Other (abiotic)	30	-5	1.10	1.28	1.47
			15	1.09	1.24	1.40
		50	-5	1.18	1.51	1.91
			15	1.15	1.43	1.75

Note: Based on Wania and Mackay[5], Anderson and Hites[24], Brubaker and Hites[25], Macdonald et al.[26]

Section S6 Phase distribution in the water column

There are many alterations to the physical environment associated with global climate change that influence organic carbon dynamics (e.g. Δ primary productivity, enhanced coastal erosion). The effect of enhanced primary productivity on actual bulk concentrations of POC and DOC in the water column of a given location will depend largely on the ratio of terrestrial to marine OC inputs in the water column (particularly in coastal regions) and the response of zooplankton grazing intensity/bacterial degradation.

Sorption to particulate and dissolved organic carbon (POC, DOC respectively) is an important consideration in the context of exposure via aquatic ecosystems because this phenomenon can have a strong influence on the freely-dissolved concentration of organic contaminants in the water column (changes in the freely-dissolved concentration are equivalent to changes in fugacity of the water compartment and bioavailability). The freely-dissolved fraction of a chemical in the water column (F_{DISS}) can be calculated as shown below[27].

$$F_{DISS} = \frac{1}{1 + K_{POC}\frac{V_{POC}}{V_W} + K_{DOC}\frac{V_{DOC}}{V_W}}$$

where K_{POC} and K_{DOC} are the POC-water and DOC-water partition coefficients respectively and V_{POC}, V_{DOC} and V_W are the volumes of POC, DOC and water in the water column (e.g. per L). The freely-dissolved fraction of organic contaminants is shown in Figure S6 as a function of K_{OC} and concentration of POC in the water column. The range of reported values of concentrations of POC in global ocean surface waters[28] is indicated as well. The concentration of DOC in the water column was assumed to be equal to POC and 10 times POC whereas the sorption capacity was assumed to be approximately 1/5th of POC (Seth et al.[29]; Burkard[30]).

As shown in Figure S6, the freely-dissolved fraction of chemicals with log $K_{OC} < 4.0$ (log $K_{OW} <$ 4.45) is similar across a wide range of POC/DOC concentrations implying low sensitivity to changes in POC/DOC concentration in the water column. Note that as a first approximation, log K_{OC} in this figure can be related to log K_{OW} values in Table S6 as log K_{OC} = log K_{OW} – 0.45[29]. For chemicals with sufficiently high log K_{OC} values, increases in POC/DOC lead to a more substantial decrease in the freely-dissolved fraction (fugacity). This response largely explains the bioaccumulation model output presented in Borgå et al.[31] (See Table 2 in main text). However, particularly during a period of primary emissions to air (i.e. fugacity in air drives distribution) there will be tendency for any decrease in the fugacity of the water column to be counteracted by enhanced net air-to-surface exchange (i.e. deposition). This is another example of compensatory behaviour; however the extent to which equifugacity between air and water is approached is a function of the exchange kinetics of the system (e.g. air-water, water-sediment, surface water-deep water). For example, in regions of high primary productivity in the ocean (e.g. 45–70 °N), strong disequilibria between air and water (f_A / f_W ratios >10) were reported for PCB-180 and a tetra- and hexachlorinated dioxin[32]. The extent of disquilibrium for these high log K_{OW} chemicals was hypothesized to reflect the depletion of the freely-dissolved phase of the water column due to the sinking flux below mixed layer depth being in excess of the atmospheric deposition flux.

This interpretation actually implies that enhanced primary productivity will only lead to greater disequilibrium ($f_W\downarrow$ in relative terms). Kinetic considerations aside, the main forcing related to increased POC/DOC in the water column is manifested as a tendency towards reduced freely-dissolved concentrations even though an increase in total water concentration (due to the additional mass of POC/DOC-associated chemical) is still possible. Exposure in pelagic food webs is reduced in scenarios with increased POC/DOC but as discussed in Macdonald et al.[26], exposure in stratified bottom waters and via the benthic food web may be impacted due to the additional mass of contaminant entering these compartments and subsequent processing in the system (e.g. POC mineralization).

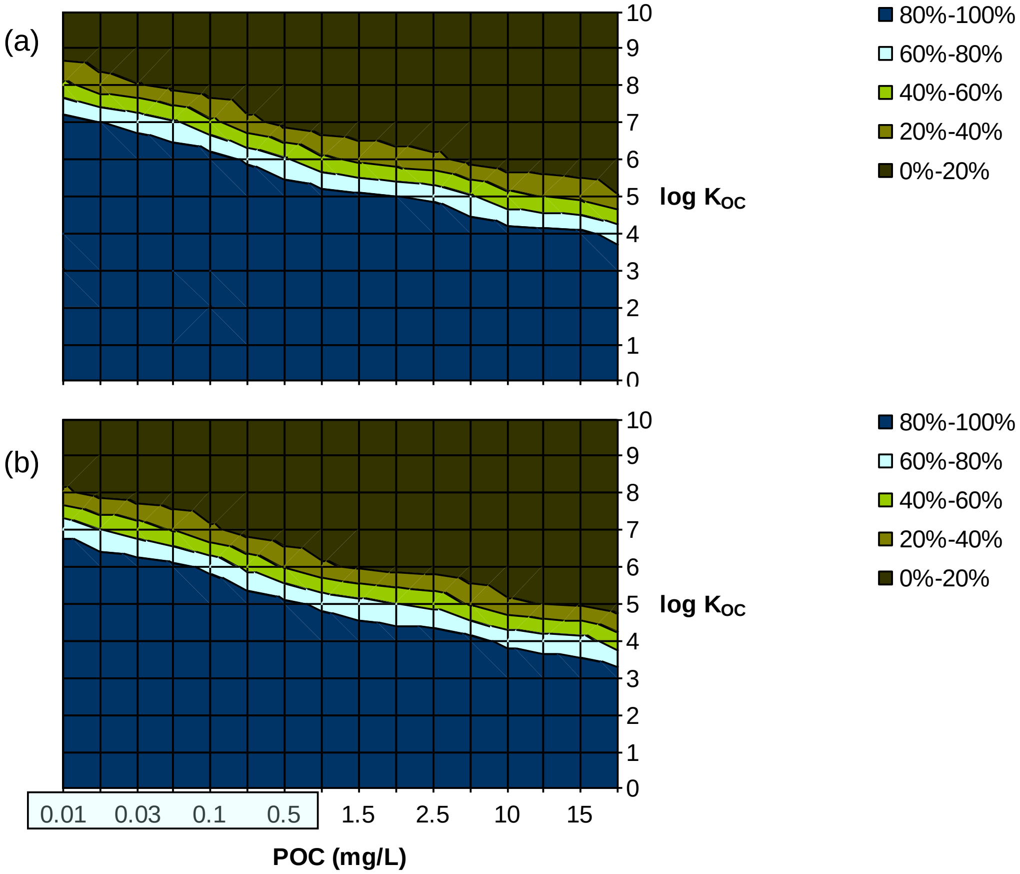

Figure S6 Freely-dissolved fraction (%) of chemical in the water column as a function of POC (and DOC) and log K_{OC}. DOC = POC in (a), DOC = 10 POC in (b). Highlighted POC equals range of values estimated for global oceans[28].

Influence of Temperature and POC/DOC

With respect to the freely-dissolved fraction in the water column, increased temperature and increased primary productivity (POC/DOC in water column) act in opposition. This compensatory behaviour is quantified in Figure S7a considering a doubling of POC/DOC and surface water temperature increases up to +8 °C (from a reference temperature of 3 °C). Calculations assuming a 10% increase in POC/DOC are shown in Figure S7b. Note that the surface water temperature in surface ocean water will not follow air temperature increases directly and also, according to the climate change projections for the Arctic[1], increases in air temperatures over open water in summer are much more limited (+1 °C) compared to winter. In winter, surface ocean temperature can be expected to be relatively stable (i.e. ~ -1.8 °C, depending on salinity) regardless.

Increase in water temperature (^{o}C)

(a)

dUoc	0	1	2	3	4	5	6	7	8
0	0.95	0.95	0.95	0.95	0.95	0.95	0.95	0.95	0.95
-10000	0.95	0.95	0.95	0.95	0.95	0.96	0.96	0.96	0.96
-20000	0.95	0.95	0.95	0.96	0.96	0.96	0.97	0.97	0.97
-30000	0.95	0.95	0.96	0.96	0.97	0.97	0.97	0.98	0.98
-40000	0.95	0.95	0.96	0.97	0.97	0.98	0.98	0.98	0.99
-50000	0.95	0.96	0.96	0.97	0.98	0.98	0.99	0.99	1.00
-60000	0.95	0.96	0.97	0.97	0.98	0.99	0.99	1.00	1.00
-70000	0.95	0.96	0.97	0.98	0.98	0.99	1.00	1.00	1.01
-80000	0.95	0.96	0.97	0.98	0.99	1.00	1.00	1.01	1.01
-90000	0.95	0.96	0.97	0.98	0.99	1.00	1.01	1.01	1.02
-100000	0.95	0.96	0.98	0.99	1.00	1.00	1.01	1.02	1.02

(b)

dUoc	0	1	2	3	4	5	6	7	8
0	0.50	0.50	0.50	0.50	0.50	0.50	0.50	0.50	0.50
-10000	0.50	0.51	0.52	0.53	0.54	0.54	0.55	0.56	0.57
-20000	0.50	0.52	0.54	0.55	0.57	0.59	0.61	0.62	0.64
-30000	0.50	0.53	0.55	0.58	0.61	0.63	0.66	0.69	0.73
-40000	0.50	0.54	0.57	0.61	0.65	0.69	0.73	0.77	0.82
-50000	0.50	0.55	0.59	0.64	0.69	0.74	0.80	0.86	0.92
-60000	0.50	0.55	0.61	0.67	0.73	0.80	0.87	0.95	1.04
-70000	0.50	0.56	0.63	0.70	0.78	0.86	0.96	1.06	1.18
-80000	0.50	0.57	0.65	0.73	0.82	0.93	1.05	1.18	1.33
-90000	0.50	0.58	0.67	0.77	0.88	1.00	1.15	1.31	1.49
-100000	0.50	0.59	0.69	0.80	0.93	1.08	1.26	1.46	1.68

Figure S7a Ratio of freely-dissolved water concentration for a chemical with (a) log K_{OC} = 4.5 and (b) log K_{OC} = 7.5 to the control scenario (no changes) as a function of the temperature-dependence of log K_{OC} (assumed equal to ΔU_{OW}) and temperature change (T_{REF} = 3 °C, +0 to 8 °C) assuming a doubling of POC/DOC in the water column. Control POC and DOC are assumed to be 0.5 and 5.0 mg/L respectively. Light blue highlighting indicates the expected range in temperature sensitivity for log K_{OC} (see Table S6). Increases in the freely-dissolved water concentration are indicated by orange shading, reductions in green.

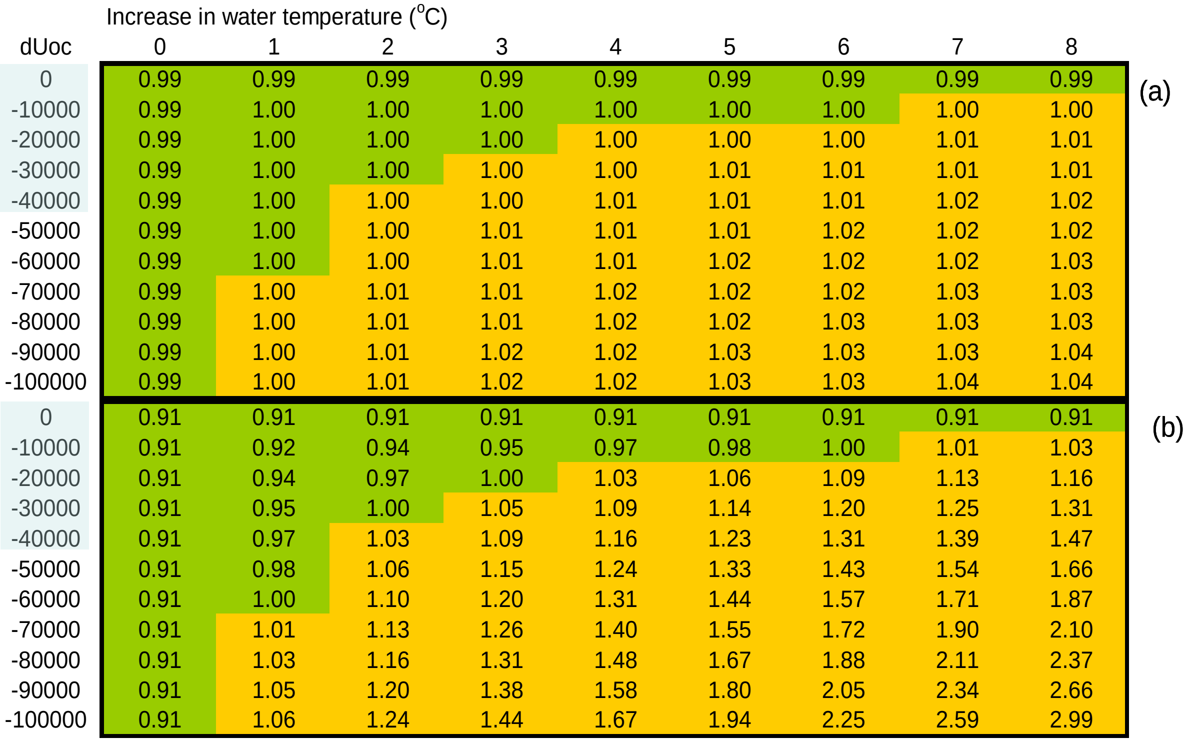

	Increase in water temperature (^{o}C)									
dUoc	0	1	2	3	4	5	6	7	8	
0	0.99	0.99	0.99	0.99	0.99	0.99	0.99	0.99	0.99	(a)
-10000	0.99	1.00	1.00	1.00	1.00	1.00	1.00	1.00	1.00	
-20000	0.99	1.00	1.00	1.00	1.00	1.00	1.00	1.01	1.01	
-30000	0.99	1.00	1.00	1.00	1.00	1.01	1.01	1.01	1.01	
-40000	0.99	1.00	1.00	1.00	1.01	1.01	1.01	1.02	1.02	
-50000	0.99	1.00	1.00	1.01	1.01	1.01	1.02	1.02	1.02	
-60000	0.99	1.00	1.00	1.01	1.01	1.02	1.02	1.02	1.03	
-70000	0.99	1.00	1.01	1.01	1.02	1.02	1.02	1.03	1.03	
-80000	0.99	1.00	1.01	1.01	1.02	1.02	1.03	1.03	1.03	
-90000	0.99	1.00	1.01	1.02	1.02	1.03	1.03	1.03	1.04	
-100000	0.99	1.00	1.01	1.02	1.02	1.03	1.03	1.04	1.04	
0	0.91	0.91	0.91	0.91	0.91	0.91	0.91	0.91	0.91	(b)
-10000	0.91	0.92	0.94	0.95	0.97	0.98	1.00	1.01	1.03	
-20000	0.91	0.94	0.97	1.00	1.03	1.06	1.09	1.13	1.16	
-30000	0.91	0.95	1.00	1.05	1.09	1.14	1.20	1.25	1.31	
-40000	0.91	0.97	1.03	1.09	1.16	1.23	1.31	1.39	1.47	
-50000	0.91	0.98	1.06	1.15	1.24	1.33	1.43	1.54	1.66	
-60000	0.91	1.00	1.10	1.20	1.31	1.44	1.57	1.71	1.87	
-70000	0.91	1.01	1.13	1.26	1.40	1.55	1.72	1.90	2.10	
-80000	0.91	1.03	1.16	1.31	1.48	1.67	1.88	2.11	2.37	
-90000	0.91	1.05	1.20	1.38	1.58	1.80	2.05	2.34	2.66	
-100000	0.91	1.06	1.24	1.44	1.67	1.94	2.25	2.59	2.99	

Figure S7b Ratio of freely-dissolved water concentration for a chemical with (a) log K_{OC} = 4.5 and (b) log K_{OC} = 7.5 to the control scenario (no changes) as a function of the temperature-dependence of log K_{OC} (assumed equal to ΔU_{OW}) and temperature change (T_{REF} = 3 °C, +0 to 8 °C) assuming a 10% increase of POC/DOC in the water column. Control POC and DOC are assumed to be 0.5 and 5.0 mg/L respectively. Light blue highlighting indicates the expected range in temperature sensitivity for log K_{OC} (see Table S6). Increases in the freely-dissolved water concentration are indicated by orange shading, reductions in green.

As can be seen by comparing Figure S7a and S7b, the magnitude of POC/DOC increase plays a strong role in whether or not warmer surface water temperatures result in enhanced or reduced freely-dissolved concentration for the more hydrophobic chemical. Assuming only a 10% increase in PP, changes in the freely-dissolved concentration are relatively minor over a realistic range of parameters (dU_{OC} from -10 to -40 000 J mol-1, temperature increase 1 to 3 ^{o}C) for both chemicals. Assuming a doubling of POC/DOC, reductions in freely-dissolved concentration are nearly proportional.

Section S7 Other examples of phase distribution calculations

1.) Influence of Salinity

Salinity has an influence on the solubility of organic contaminants in the water phase and hence also influences air-water partitioning and partitioning to organic phases in the aqueous environment (see Xie and Mackay[33]). The influence of salt content on solubility of neutral organic compounds is typically described using the Setschenow equation[34].

$$\log \frac{S}{S_O} = -K_S C_S$$

where S is the solubility of the compound in the salt solution, S_O is the solubility in pure water, K_S is the empirical Setschenow constant and C_S is the molar concentration of the electrolytes in solution. Ni and Yalkowsky[35] recently proposed the following relationship between K_S and log K_{OW}.

$$K_S = 0.040 \cdot \log K_{OW} + 0.114$$

Using these two equations, the ratio in solubilities at different molar concentrations of sodium chloride is shown in Table S8 as a function of K_{OW}

Table S8 Ratio of solubilities and comparison of log K_{OW} values at different salinities.

Log K_{OW}	K_S	S/S_O				Log K_{OW}	
(0 M)		C_S = 0 M	0.1 M	0.3 M	0.5 M	0.1 M	0.5 M
1.0	0.154	1.00	0.97	0.90	0.84	1.02	1.08
2.0	0.194	1.00	0.96	0.87	0.80	2.02	2.10
3.0	0.234	1.00	0.95	0.85	0.76	3.02	3.12
4.0	0.274	1.00	0.94	0.83	0.73	4.03	4.14
5.0	0.314	1.00	0.93	0.81	0.70	5.03	5.16
6.0	0.354	1.00	0.92	0.78	0.67	6.04	6.18
7.0	0.394	1.00	0.91	0.76	0.64	7.04	7.20
8.0	0.434	1.00	0.90	0.74	0.61	8.04	8.22
9.0	0.474	1.00	0.90	0.72	0.58	9.05	9.24
10.0	0.514	1.00	0.89	0.70	0.55	10.05	10.26

As shown in Table S8, the maximum reduction in the solubility of neutral organic compounds in sea water versus pure water is approximately a factor of two. These results are consistent with the magnitude of change estimated by Xie and Mackay[33]. While salinity effects are worth quantifying when parameterizing fate/transport and bioaccumulation models for freshwater compared to marine environments, the magnitude of changes in salinity linked to global climate change (e.g. enhanced river discharge) are not likely to alter the solubility (and other partition coefficients and fate processes) of neutral organic compounds to a great extent. For example, a 20% reduction in salinity from 0.5 to 0.4 M results in an increase in solubility of only 2–12%. With respect to phase distribution, food-web accumulation and human exposure, these changes are not likely to be important in comparison to other changes.

2.) Aerosol-air partitioning

There are numerous approaches for estimating partition coefficients between aerosols and the gas phase[27,36,37]. A volumetric partition coefficient (K_{QA}, m^3 air m^{-3} aerosol) is the most convenient for environmental fate modeling. Once K_{QA} is estimated, the fraction of contaminant associated with aerosols as opposed to being in the gas phase (φ) can be estimated as shown below.

$$\varphi = \frac{K_{QA} v_Q}{(1 + K_{QA} v_Q}$$

where v_Q is the volume fraction of aerosol in the atmosphere. A typical value[36] in non-urban area $= 2 \cdot 10^{-11}$. The fraction of contaminant mass associated with aerosols is shown as a function of K_{QA} and aerosol volume fraction in Figure S8.

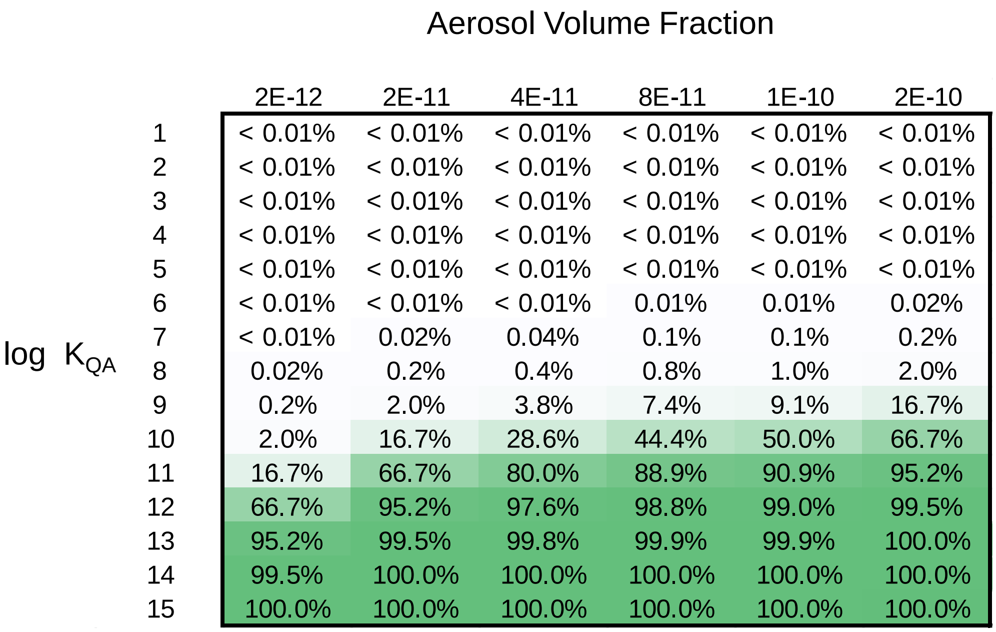

Aerosol Volume Fraction

log K_{QA}	2E-12	2E-11	4E-11	8E-11	1E-10	2E-10
1	< 0.01%	< 0.01%	< 0.01%	< 0.01%	< 0.01%	< 0.01%
2	< 0.01%	< 0.01%	< 0.01%	< 0.01%	< 0.01%	< 0.01%
3	< 0.01%	< 0.01%	< 0.01%	< 0.01%	< 0.01%	< 0.01%
4	< 0.01%	< 0.01%	< 0.01%	< 0.01%	< 0.01%	< 0.01%
5	< 0.01%	< 0.01%	< 0.01%	< 0.01%	< 0.01%	< 0.01%
6	< 0.01%	< 0.01%	< 0.01%	0.01%	0.01%	0.02%
7	< 0.01%	0.02%	0.04%	0.1%	0.1%	0.2%
8	0.02%	0.2%	0.4%	0.8%	1.0%	2.0%
9	0.2%	2.0%	3.8%	7.4%	9.1%	16.7%
10	2.0%	16.7%	28.6%	44.4%	50.0%	66.7%
11	16.7%	66.7%	80.0%	88.9%	90.9%	95.2%
12	66.7%	95.2%	97.6%	98.8%	99.0%	99.5%
13	95.2%	99.5%	99.8%	99.9%	99.9%	100.0%
14	99.5%	100.0%	100.0%	100.0%	100.0%	100.0%
15	100.0%	100.0%	100.0%	100.0%	100.0%	100.0%

Figure S8 Fraction of contaminant associated with aerosols as a function of K_{QA} and aerosol volume fraction.

Under typical conditions (i.e. outside of urban areas), log K_{QA} must be ≥ 9 at the ambient environmental temperature before the mass fraction associated with aerosols is significant. Assuming K_{QA} can be estimated as a first approximation as 0.13 K_{OA}[38], this threshold in distribution behaviour corresponds to log $K_{OA} \geq 9.9$ (at ambient environmental temperature). Below this value, fate processes related to the gas phase are dominant (e.g. diffusive air-to-surface exchange > wet particle deposition & dry particle deposition). Chemicals with log $K_{QA} \geq 13$ (log $K_{OA} \geq 13.9$) at the ambient environmental temperature are almost entirely associated with aerosols and fate processes related to the particle phase are key.

Influence of temperature changes on aerosol-air partitioning

In the context of global climate change, warmer temperatures correspond to a higher mass fraction in the gas phase. Such shifts in K_{QA} due to temperature change can be important in relative terms at the extremes of the mass distribution. For example, if a chemical moves from being 95% associated with aerosols to 70%, the fraction in the gas phase has increased 6-fold (5% to 30%). Such a shift could have important implications with respect to the importance of gas phase degradation in overall fate and transport. The ratio of the mass fraction in the gas phase under warmer conditions versus the default scenario as a function of temperature increase and temperature-dependence of K_{QA} is shown in Figure S9.

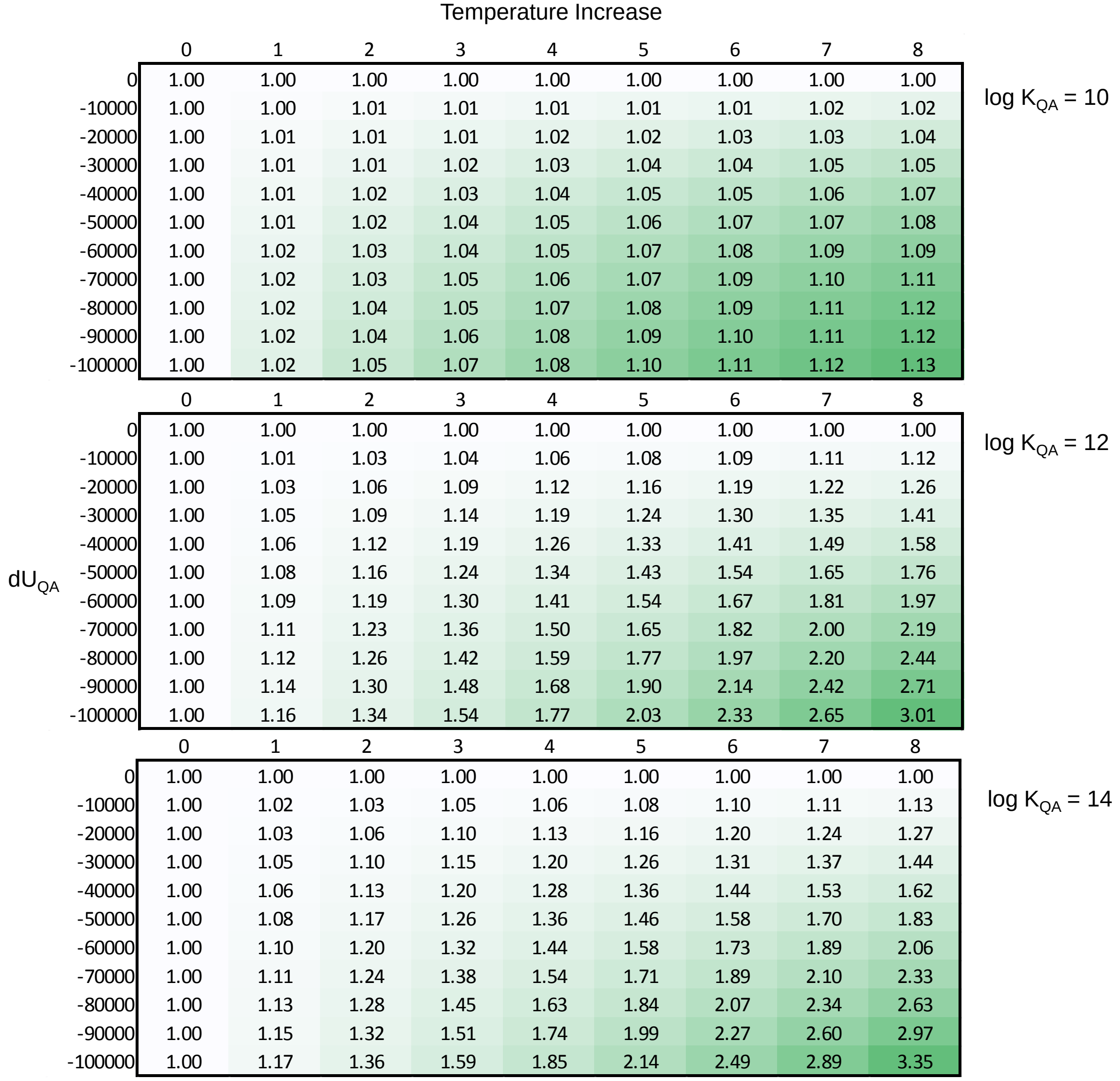

Temperature Increase

dU$_{QA}$

	0	1	2	3	4	5	6	7	8
0	1.00	1.00	1.00	1.00	1.00	1.00	1.00	1.00	1.00
-10000	1.00	1.00	1.01	1.01	1.01	1.01	1.01	1.02	1.02
-20000	1.00	1.01	1.01	1.01	1.02	1.02	1.03	1.03	1.04
-30000	1.00	1.01	1.01	1.02	1.03	1.04	1.04	1.05	1.05
-40000	1.00	1.01	1.02	1.03	1.04	1.05	1.05	1.06	1.07
-50000	1.00	1.01	1.02	1.04	1.05	1.06	1.07	1.07	1.08
-60000	1.00	1.02	1.03	1.04	1.05	1.07	1.08	1.09	1.09
-70000	1.00	1.02	1.03	1.05	1.06	1.07	1.09	1.10	1.11
-80000	1.00	1.02	1.04	1.05	1.07	1.08	1.09	1.11	1.12
-90000	1.00	1.02	1.04	1.06	1.08	1.09	1.10	1.11	1.12
-100000	1.00	1.02	1.05	1.07	1.08	1.10	1.11	1.12	1.13

log K_{QA} = 10

	0	1	2	3	4	5	6	7	8
0	1.00	1.00	1.00	1.00	1.00	1.00	1.00	1.00	1.00
-10000	1.00	1.01	1.03	1.04	1.06	1.08	1.09	1.11	1.12
-20000	1.00	1.03	1.06	1.09	1.12	1.16	1.19	1.22	1.26
-30000	1.00	1.05	1.09	1.14	1.19	1.24	1.30	1.35	1.41
-40000	1.00	1.06	1.12	1.19	1.26	1.33	1.41	1.49	1.58
-50000	1.00	1.08	1.16	1.24	1.34	1.43	1.54	1.65	1.76
-60000	1.00	1.09	1.19	1.30	1.41	1.54	1.67	1.81	1.97
-70000	1.00	1.11	1.23	1.36	1.50	1.65	1.82	2.00	2.19
-80000	1.00	1.12	1.26	1.42	1.59	1.77	1.97	2.20	2.44
-90000	1.00	1.14	1.30	1.48	1.68	1.90	2.14	2.42	2.71
-100000	1.00	1.16	1.34	1.54	1.77	2.03	2.33	2.65	3.01

log K_{QA} = 12

	0	1	2	3	4	5	6	7	8
0	1.00	1.00	1.00	1.00	1.00	1.00	1.00	1.00	1.00
-10000	1.00	1.02	1.03	1.05	1.06	1.08	1.10	1.11	1.13
-20000	1.00	1.03	1.06	1.10	1.13	1.16	1.20	1.24	1.27
-30000	1.00	1.05	1.10	1.15	1.20	1.26	1.31	1.37	1.44
-40000	1.00	1.06	1.13	1.20	1.28	1.36	1.44	1.53	1.62
-50000	1.00	1.08	1.17	1.26	1.36	1.46	1.58	1.70	1.83
-60000	1.00	1.10	1.20	1.32	1.44	1.58	1.73	1.89	2.06
-70000	1.00	1.11	1.24	1.38	1.54	1.71	1.89	2.10	2.33
-80000	1.00	1.13	1.28	1.45	1.63	1.84	2.07	2.34	2.63
-90000	1.00	1.15	1.32	1.51	1.74	1.99	2.27	2.60	2.97
-100000	1.00	1.17	1.36	1.59	1.85	2.14	2.49	2.89	3.35

log K_{QA} = 14

Figure S9 Ratio of the mass fraction in the gas phase under warmer conditions versus the default scenario as a function of temperature increase and temperature-dependence of K_{QA} assuming a reference temperature of 5 °C, an aerosol volume fraction of $2\cdot10^{-11}$ and default log K_{QA} (i.e. at 5 °C) values of 10, 12 and 14.

As shown in Figure S9, the mass fraction of contaminant in the gas phase is relatively insensitive to warmer temperatures when log K_{QA} = 10 across the range of ΔU_{QA} and temperature increase. More substantial shifts are seen for the other two examples (i.e. up to a factor of ~ 3.5). In the context of atmospheric degradation, these ratios reflect the maximum possible influence on air concentrations (i.e. factor of change ↓ assuming that degradation is the dominant fate process determining these levels). Fate and transport calculations are required to assess the associated change for contaminants where other fate processes have a substantial influence on determining air concentrations.

Section S8 Examples of process-specific rate constant calculations

1.) Atmospheric degradation

Atmospheric degradation is a function of both temperature and concentration of reactants (e.g. OH radicals). Reaction with OH radicals is often the most important atmospheric degradation pathway for organic contaminants[39] and the pseudo-first order rate constant for this reaction is calculated as shown below.

$$k_{DEG} = k_{OH}[OH]$$

where k_{OH} is the second order reaction rate constant for the chemical (cm^3 molecule^{-1} s^{-1}) and [OH] is the concentration of OH radicals in the atmosphere (molecules cm^{-3}). This reaction is typically assumed to apply only to the fraction of contaminant in the gas phase. Empirical k_{OH}s for organic chemicals[40-42] range between 10^{-10} to 10^{-15} whereas most Arctic contaminants have estimated k_{OH}s in the range of 10^{-12} to 10^{-14}. Based on [OH] estimated presented in Bahm and Kahil[43], baseline half-lives due to reaction with OH radicals at temperate and northern latitudes are presented in Table S9.

Table S9 Estimated half-lives (HL, d) due to gas phase reactions with OH radicals as a function of OH radical rate constant and concentration of OH radicals (molecules cm^{-3}) at a temperate and northern latitude.

k_{OH} (cm^3 molecule^{-1} s^{-1})	HL (d) at 45 °N, summer [OH] = 14.9 x 10^5	HL (d) at 85 °N, summer [OH] = 6.3 x 10^5
10^{-10}	0.05	0.13
10^{-11}	0.5	1.3
10^{-12}	5.4	12.7
10^{-13}	54	127
10^{-14}	540	1270
10^{-15}	5400	12700

Any changes in [OH] result in a proportional change in the HL whereas changes in temperature result in non-linear changes in k_{OH} (and also the fraction of chemical in the gas phase). As an example, assuming an activation energy for OH radical reactions of 10 kJ mol^{-1} (see Anderson and Hites[24]; Brubaker and Hites[25]), an increase in air temperature of 5 °C (using 15 °C as baseline) corresponds to an increase in k_{OH} of approximately 10%. This response represents the extent to which temperature can compensate possible reductions in [OH] due to elevated levels of carbon monoxide and methane, should they occur[44]. Overall, given the relatively low temperature-dependence of OH reactions and stability of [OH] at the global scale over the past century[45], global climate change is not likely to have a substantial influence on this process.

2.) Precipitation scavenging

Deposition of contaminants with precipitation can be separated into two processes, wet gaseous deposition (i.e. rain dissolution) and wet particle deposition. Both processes are quantified using partition coefficients and precipitation rate. The rate constant associated with each process (k, h^{-1}) can be estimated using mass transfer coefficients (MTC, m h^{-1}), i.e.

$$k_{WG} = \frac{MTC_{WG}}{h}$$

where h is the height of the atmosphere (m) assumed for the calculation. Approaches for estimating these MTCs as well as an approximation to account for the intermittent nature of precipitation were recently summarized in the Handbook of Chemical Mass Transport in the Environment[38].

The MTCs for wet gaseous deposition (WG) and wet particle deposition (WP) are shown below:

$$MTC_{WG} = \frac{U_R(1-\varphi)}{(K_{AW} + V_R / V_A)}$$

$$MTC_{WP} = U_R Q \varphi$$

where U_R is the precipitation rate (default = 9.7×10^{-5} m h^{-1}, 850 mm yr^{-1}), Q is the particle scavenging efficiency (default = 50 000), φ is the fraction of contaminant associated with aerosols and V_R / V_A is the volume ratio of rain drops to air (default = 6×10^{-8}). φ can be calculated using the volume fraction of aerosols in the atmosphere (default = $2 \cdot 10^{-11}$) and the aerosol-air partition coefficient K_{QA}. For the calculations presented here, K_{QA} was estimated as a first approximation from K_{OA} using the following expression[38], i.e.,

$$K_{QA} = 0.13 K_{OA}$$

The limit imposed to the maximum wet deposition MTC based on the intermittent rain approximation is calculated as shown below.

$$MTC_{MAX} = \frac{2h(t_{DRY} + t_{WET})}{t_{DRY}^2}$$

where h is the height of the atmosphere (default = 1000 m), t_{DRY} is the average period of time with no precipitation (default = 120 h) and t_{WET} is the average length of a precipitation event (default = 12 h).

Atmospheric half-lives due to precipitation scavenging (rain dissolution + wet particle deposition, incorporating an intermittent rain approximation) as a function of K_{AW} and K_{OW} are presented in Figure S10.

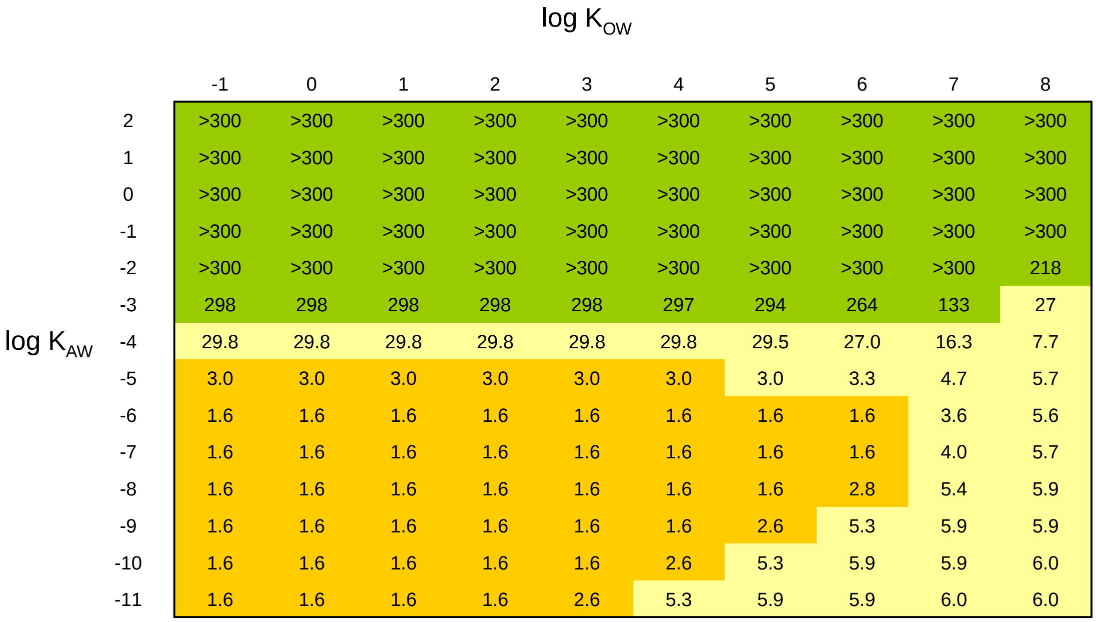

log K_{OW}

log K_{AW}	-1	0	1	2	3	4	5	6	7	8
2	>300	>300	>300	>300	>300	>300	>300	>300	>300	>300
1	>300	>300	>300	>300	>300	>300	>300	>300	>300	>300
0	>300	>300	>300	>300	>300	>300	>300	>300	>300	>300
-1	>300	>300	>300	>300	>300	>300	>300	>300	>300	>300
-2	>300	>300	>300	>300	>300	>300	>300	>300	>300	218
-3	298	298	298	298	298	297	294	264	133	27
-4	29.8	29.8	29.8	29.8	29.8	29.8	29.5	27.0	16.3	7.7
-5	3.0	3.0	3.0	3.0	3.0	3.0	3.0	3.3	4.7	5.7
-6	1.6	1.6	1.6	1.6	1.6	1.6	1.6	1.6	3.6	5.6
-7	1.6	1.6	1.6	1.6	1.6	1.6	1.6	1.6	4.0	5.7
-8	1.6	1.6	1.6	1.6	1.6	1.6	1.6	2.8	5.4	5.9
-9	1.6	1.6	1.6	1.6	1.6	1.6	2.6	5.3	5.9	5.9
-10	1.6	1.6	1.6	1.6	1.6	2.6	5.3	5.9	5.9	6.0
-11	1.6	1.6	1.6	1.6	2.6	5.3	5.9	5.9	6.0	6.0

Figure S10 Half-life in the atmosphere (days) due to precipitation (rain dissolution + wet particle deposition, incorporating an intermittent rain approximation) as a function of K_{AW} and K_{OW} assuming a precipitation rate of 850 mm yr^{-1}

With respect to atmospheric long-range transport potential, the value of Figure S10 is that it identifies range of physical-chemical properties where the influence of precipitation increases in the range of 10–35% is negligible (log K_{AW} 2 to –3, log K_{OW} -1 to 7) because precipitation scavenging is inefficient; where precipitation scavenging is highly efficient, a proportional decrease in long-range transport can be expected. Further details on calculating MTCs for precipitation and many other fate processes are provided in the Handbook of Chemical Mass Transport in the Environment[38].

Section S9 Arctic Contamination Potential ($eACP_{10}$)

The Arctic Contamination Potential ($eACP_{10}$) is calculated as shown below[46].

$$eACP_{10} = \frac{M_{AS}}{M_{GE}}$$

where M_{AS} is the mass of contaminant in the surface compartments of the Arctic environment (i.e. excluding air) and M_{GE} is the total mass of contaminant emitted into the global environment over the simulation (typically 10 years). An Arctic Contamination Potential specific to the marine environment could simply be calculated as:

$$eACP_{Ocean10} = \frac{M_{AO}}{M_{GE}}$$

where M_{AO} is the mass of contaminant in the surface layer of the Arctic marine environment. In the default calculation, emissions are distributed spatially according to population density.

List of parameters included in sensitivity analysis of $eACP_{10}$ (see Meyer & Wania[47])

Organic carbon fraction in uncultivated soil
Organic carbon fraction in ocean suspended solids
Suspended solid volume fraction in ocean waters

Depth of uncultivated soil
Depth of surface ocean compartment (i.e. mixed layer depth)

Aerosol volume fraction in atmosphere
Organic matter content of aerosols
Particle scavenging ratio

Fraction of water in soil pore space
Fraction of air in soil pore space

Rain rate over continents
Rain rate over oceans
Mass transfer coefficient between air and water (air-side)
Mass transfer coefficient between air and water (water-side)
Mass transfer coefficient between soil and air (air-side)
Dry deposition velocity over continents
Dry deposition velocity over oceans
Solid-phase diffusion in soil

Horizontal atmospheric macro-diffusion coefficient
Vertical atmospheric macro-diffusion coefficient
Horizontal atmospheric advection coefficient

Sea ice cover (%)
Temperature

Section S10 Comparison of atmospheric deposition MTCs and half-lives for PCBs in the Arctic at -20 °C and -10 °C

Sorption to falling snow (i.e. snowflake-air partitioning)

Adsorption to the surface of snow (K_{SA}) can be estimated using a polyparameter linear free energy relationship (ppLFER) provided in Roth et al.[48].

$$\log K_{SA}(-6.8^{o}C) = 0.639 \cdot \log K_{HXA} + 3.53 \cdot \sum\alpha + 3.38 \cdot \sum\beta - 6.85$$

where K_{HXA} is the hexadecane-air partition coefficient (at 25 °C) and $\Sigma\alpha$ and $\Sigma\beta$ characterize electron acceptor and donor ability, respectively.

Approaches for estimating temperature-dependence of interface-air partition coefficients (K_{iA}) were proposed in Goss & Schwarzenbach[49] and Roth et al.[50] where the temperature dependence of the partition coefficient is estimated using an empirically-based regression. Equations used in Lei and Wania[51] were applied here, as shown below.

$$\log K_{iA}(15^{o}C) = 0.635 \cdot \log K_{HXA} + 3.60 \cdot \sum\alpha + 5.11 \cdot \sum\beta - 8.47$$

$$\Delta U_{iA} = -5.07 \ln K_{IA}(15^{o}C) - 108$$

where ΔU_{iA} is in units of kJ mol^{-1}. Under this approach, it is assumed that ΔU_{iA} is constant over the entire range of temperatures considered.

The units of K_{SA} calculated above are m^3 air m^{-2} snow surface. This partition coefficient can be converted to a volumetric partition coefficient (i.e. m^3 air m^{-3} snow surface) using the following expression.

$$K_{SA}^{VOL} = K_{SA} \cdot SSA_F \cdot \rho_F$$

where SSA_F is the specific surface area of the snowflake (m^2 kg^{-1}) and ρ_F is the density of the snowflake (kg m^{-3}). Typical values for SSA_F and ρ_F are 100 m$_2$ kg^{-1} and 920 kg m^{-3} respectively[38]. Solvation parameters and K_{IA} for PCB congeners are compiled in Table S10; snow-air partition coefficients are shown in Table S11.

Table S10 Solvation parameters and interface-air partition coefficients for PCBs.

Congener	K_{HXA}	$\Sigma\alpha$	$\Sigma\beta$	log K_{IA} (m^3 m^{-2})	ΔU_{IA} (kJ mol^{-1})
PCB-28	7.904	0	0.15	-2.68	-76.7
PCB-52	8.144	0	0.15	-2.53	-78.4
PCB-101	8.868	0	0.13	-2.17	-82.6
PCB-118	9.396	0	0.11	-1.94	-85.3
PCB-138	9.772	0	0.11	-1.70	-88.1
PCB-153	9.587	0	0.11	-1.82	-86.6
PCB-180	10.415	0	0.09	-1.39	-91.7

Table S11 Snowflake-air partition coefficients for PCBs at -20 and -10 °C and the associated factor of change.

Congener	Log K_{SA}(-6.8 °C) ($m^3\ m^{-2}$)	Log K_{SA}(-6.8 °C) ($m^3\ m^{-3}$)	Log K_{SA} (-20 °C)	Log K_{SA} (-10 °C)	Ratio (-20 ^{o}C : -10 ^{o}C)
PCB-28	-1.29	3.67	4.45	3.85	4.0
PCB-52	-1.14	3.82	4.62	4.01	4.1
PCB-101	-0.74	4.22	5.06	4.42	4.4
PCB-118	-0.47	4.49	5.36	4.69	4.6
PCB-138	-0.23	4.73	5.63	4.94	4.9
PCB-153	-0.35	4.61	5.50	4.82	4.8
PCB-180	0.11	5.07	6.01	5.29	5.2

Aerosol-air Partitioning in the Arctic

As described above, K_{QA} can be estimated from K_{OA} as a first approximation assuming that $K_{QA} = 0.13\ K_{OA}$. This relationship is based on a set of default assumptions so it is now useful to present this approximation in more generic terms, as shown below.

$$K_{QA} = B \cdot K_{OA}$$

$$B = f_{OM} \frac{\rho_Q}{\rho_O} \frac{M_O}{M_{OM}} \frac{\gamma_O}{\gamma_{OM}}$$

where f_{OM} is the mass fraction of organic matter in aerosol, ρ_Q is the assumed density of the aerosol (2000 kg m^{-3}), ρ_O is the density of octanol (840 kg m^{-3}), M_O and M_{OM} are the molecular mass of octanol and aerosol organic matter, respectively, γ_O and γ_{OM} are the activity coefficient of the chemical in octanol and organic matter, respectively. When M_O / M_{OM} is assumed to equal 0.26, γ_O / γ_{OM} = 1 and f_{OM} assumed to be 0.2, B = 0.13[38]. Based on empirical data collected at Alert in the Canadian Arctic[52,53], f_{OM} was assumed to be 0.07 for aerosol-air calculations in the Arctic, corresponding to B = 0.043. Aerosol-air partition coefficients at -20 and -10 °C are shown in Table S12.

Table S12 Arctic aerosol-air partition coefficients for PCBs at 15, -20 and -10 °C and the factor of change between partition coefficients at -20 and -10 °C

Congener	ΔU_{OA} (kJ mol^{-1})	Log K_{QA}(15 °C) ($m^3\ m^{-3}$)	Log K_{QA} (-20 °C)	Log K_{QA} (-10 °C)	Ratio (-20 ^{o}C : -10 ^{o}C)
PCB-28	-78.4	6.99	8.95	8.34	4.1
PCB-52	-81.3	7.36	9.40	8.76	4.3
PCB-101	-84.4	7.99	10.11	9.45	4.6
PCB-118	-89.8	8.64	10.89	10.18	5.1
PCB-138	-86.9	8.85	11.03	10.35	4.8
PCB-153	-94.8	8.68	11.05	10.31	5.5
PCB-180	-95.2	9.40	11.79	11.04	5.6

Mass Transfer Coefficients

The fraction of chemical in the gas phase (φ) is calculated as shown previously (i.e. as a function of aerosol-air partitioning and volume fraction of aerosols); the default assumption for aerosol volume fraction in the Arctic was $2\cdot10^{-11}$.

The MTC for snow dissolution (SG) is calculated similarly to the MTC for rain dissolution.

$$MTC_{SG} = \frac{U_S(1-\varphi)}{(\frac{1}{K_{SA}^{VOL}} + V_S/V_A)}$$

where U_S is the snow precipitation rate and V_S/V_A is the volume ratio of snow to air in the atmosphere. Default values were $5.3\cdot10^{-5}$ m h^{-1} and $6\cdot10^{-8}$ for U_S and V_S/V_A respectively

The MTC for wet particle deposition (WP) is also analogous to that for rainfall.

$$MTC_{WP} = U_S Q\varphi$$

The default value for Q was 50000.

An additional MTC describing dry deposition is required for this analysis. Following the Handbook of Chemical Mass Transport in the Environment[38], this MTC is estimated as,

$$MTC_{DP} = U_D\varphi$$

where U_D is the dry particle settling rate, here given a default value of 4.6 m h^{-1}.

Half-lives associated with each transport process can then be estimated as shown below

$$HL = \ln(2)\frac{h}{MTC_i}$$

where h is the assumed height of the atmosphere (1000 m).

A comparison atmospheric half-lives at -20 and -10 °C is summarized in Table S13, while a comparison of the different MTCs at -20 and -10 °C is presented in Figure S11.

Table S13 Overall atmospheric half-life (d) due to dry particle deposition and snowfall at -20 °C and -10 °C for selected PCBs.

Congener	At -20 °C	At -10 °C	Factor
PCB-28	18.0	70.6	3.9
PCB-52	11.7	46.4	4.0
PCB-101	4.6	17.0	3.7
PCB-118	3.2	7.8	2.5
PCB-138	2.4	5.3	2.2
PCB-153	2.9	6.3	2.2
PCB-180	2.7	3.5	1.3

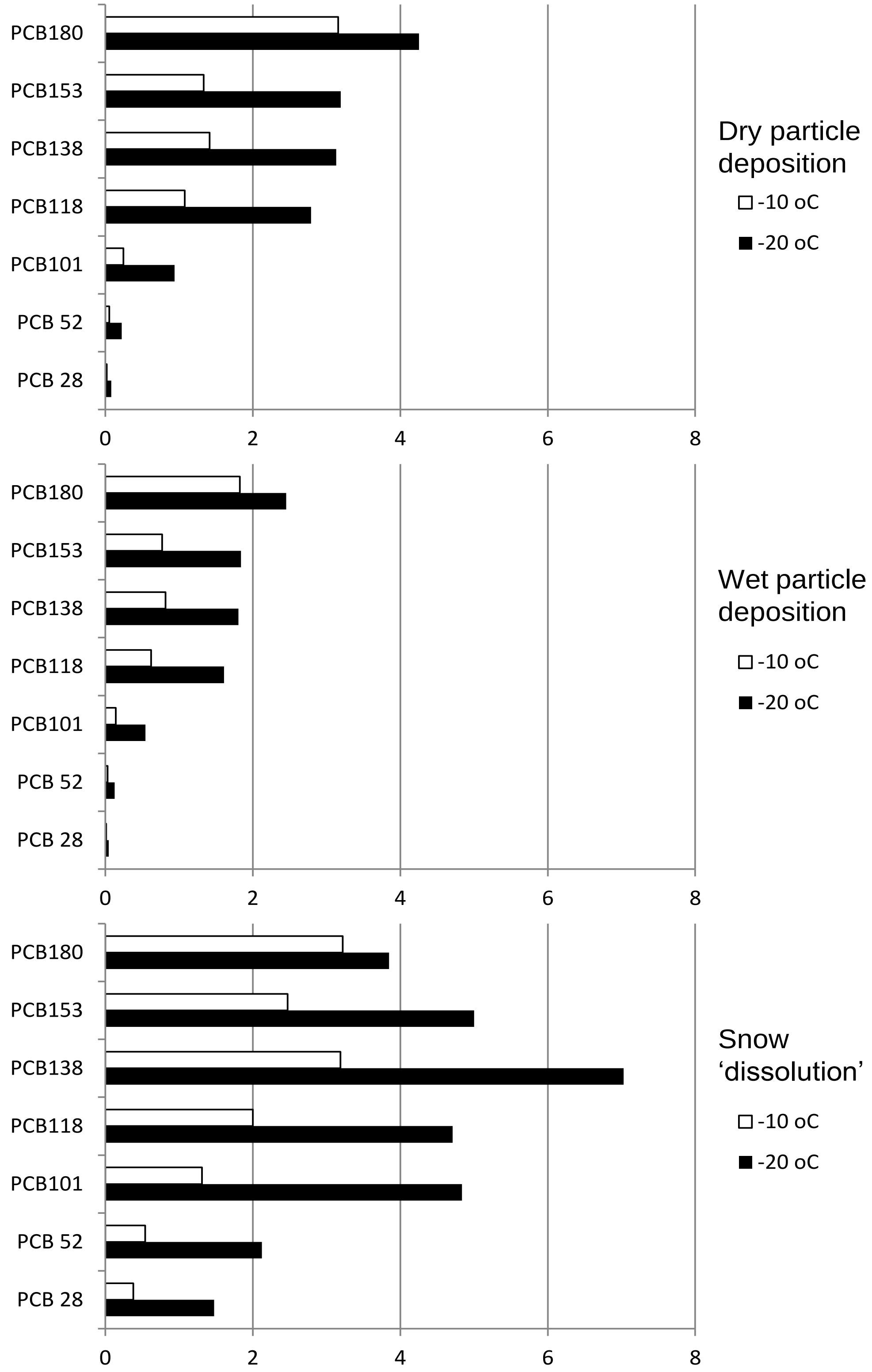

Figure S11 Mass transfer coefficients (m h^{-1}) at -20 °C and -10 °C for dry particle deposition, wet particle deposition and snow 'dissolution' for different PCBs

Section S11 Increased frequency of forest fires

Numerous studies have investigated the potential implications of global climate change on the frequency of forest fires in boreal regions[54-58]. Outputs from general circulation models (GCMs) can be used to estimate indices such as the Fire Weather Index (FWI), which is a function of temperature, relative humidity, wind speed and precipitation. Using such approaches, the area burned in Canada was estimated to increase 74–118% by the year 2100 assuming a 3 x CO_2 scenario[57]. There is substantial spatial variability and uncertainty in these estimates due to the complex interactions of direct climate changes (e.g. temperature, precipitation) and indirect changes (e.g. vegetation shifts, incidence of insect infestation) on forest fire frequency. Regardless, the general consensus is that increased fire frequency, fire season length and/or severity can be expected in the boreal region overall under a warmer climate.

Emissions of certain contaminants (PAHs, dioxins/furans, PCBs, PBDEs) during burning events have also been studied in different situations[59-62] in order to derive emission factors (EF in g chemical kg^{-1} material burned). In the context of forest fires, chemicals can be divided into three categories, i) those that are released primarily due to production during combustion (e.g. PAHs) ii) those that are released primarily due to enhanced revolatilization from soil reservoirs (e.g. PCBs) and iii) those that can be released both ways. In order to put this global climate change effect into perspective, it is necessary to first estimate emissions due to forest fires under current conditions in relation to other emission sources. An example using data for PCBs is presented here given the availability of required inputs and also the recent observations linking boreal forest fires with record high peak PCB concentrations measured at the Zeppelin station on Svalbard in 2004 and 2006[63].

Emissions of contaminants due to forest fires can be estimated as shown below.

$$M_{FF} = EF \cdot D_B \cdot A_{FF}$$

where D_B is the biomass density (kg m^{-2}) and A_{FF} is the area burned (m^2). Biomass density in boreal forests is variable spatially, ranging from 1.0–10.8 kg dry m^{-2} with an average value of 4.2 kg dry m^{-2} in one field-based study[64]. This range in estimates is consistent with values presented in Fang et al.[65] For PCBs, the emission factors predominantly represent revolatilization from soils during and after a forest fire[63] and hence are likely to be dependent on the soil concentration. The dependence of the apparent *EF* on soil concentration introduces uncertainty to the emission estimates for current and future assessments because of both spatial variation[66] and temporal change in PCB levels (i.e. dissipation over time). Nevertheless, example calculations of emissions per million ha burned are presented in Table S14 for seven PCB congeners.

Estimates of average annual area of burn for Russian boreal forests vary substantially among sources (partly due to reporting issues) but it is likely in the range of 7–10 million ha whereas the long-term average annual area burn is 1.6 million ha in Canada (1920–2006) and 0.4 million ha in Alaska (1950-2006)[58,67,68]. Assuming an average annual burn area of 10 million ha for all boreal forests, the emission factors estimated by Eckhardt et al.[63] result in substantial annual emissions, particularly for the lower chlorinated PCBs. A comparison between emissions due to boreal forest fires (assuming average biomass density) and those estimated for primary sources for 2004-2006[6] is shown in Table S15.

Table S14 Apparent emission factors[63] and emissions per 10^6 ha of forest burned (kg) for seven PCB congeners assuming an average boreal forest dry biomass density[64] of 4.2 (1.0–10.8) kg dry m^{-2}

Compound	EF_A 2004* µg kg^{-1} dry	Emissions per 10^6 ha burned (kg)	EF_A 2006* µg kg^{-1} dry	Emissions per 10^6 ha burned (kg)
PCB-28	28	1180 (280 – 3025)	10	435 (105 – 1120)
PCB-52	9.7	405 (100 – 1040)	4.4	180 (45 – 470)
PCB-101	3.3	140 (30 – 350)	2.2	90 (20 – 240)
PCB-118	0.88	40 (10 – 95)	1.8	75 (20 – 190)
PCB-138	0.67	30 (7 – 70)	1.4	60 (15 – 155)
PCB-153	0.88	40 (9 – 95)	2.1	90 (20 – 230)
PCB-180	0.16	7.0 (2 – 18)	0.33	14 (3 – 35)

*Note that the EFs presented in Table S14 are expected to have uncertainty range of a factor of 2-3 in either direction[63]. This uncertainty will increase the range in emissions per 10^6 ha beyond what is shown here (only includes uncertainty in dry biomass density)

Table S15 Comparison of estimated emissions (t yr^{-1}) from primary sources[6] and boreal forest fires for seven PCB congeners for the period 2004–2006

Compound	Estimated Emissions: Primary Sources* (2004 – 2006) t yr^{-1}	Estimated Emissions: Boreal Forest Fires (10 million Ha burned) t yr^{-1}
PCB-28	34 – 40	4 – 12
PCB-52	18 – 21	2 – 4
PCB-101	9 – 11	0.9 – 1.4
PCB-118	12 – 15	0.4 – 0.8
PCB-138	9 – 11	0.3 – 0.6
PCB-153	10 – 13	0.4 – 0.9
PCB-180	3 – 4	0.07 – 0.14

* values from ‘high’ emission scenario used; ‘mid’ scenario is ~ 20- to 40-fold lower, which would imply forest fires as a dominant source in comparison.

While these calculations are intended to be more illustrative, it is interesting to note that the results support the notion that boreal forest fires can influence the contemporary atmospheric burden of PCB-28 and 52 on a global scale (particularly during years of enhanced burning)[63,69]. The relevance of these emissions in the long-term depends on the dissipation half-life of PCBs in boreal forest soils compared to how primary emissions of PCBs evolve over time. Even with a doubling of the area burned however, it seems unlikely that PCB emissions will ever approach estimated historic maximums (e.g. ~ 400 and 200 *t* yr^{-1} for PCB-52 and 28 respectively)[6]. Regardless, the relationship between boreal forest fires and atmospheric levels of PCBs deserves further consideration in terms of variability in monitoring data from the past two decades into the near-future. For all contaminants which are emitted primarily as a result of revolatilization from soils, the EFs will likely depend on the soil concentration and resistance to thermal degradation; further research into contaminants of interest is required.

<u>Section S12</u> Shift northward in emissions/use of chemicals

Assuming the same spatial distribution and circulation patterns, change in the magnitude of emissions can be expected to result in a proportional change in environmental fugacities in remote regions (and hence exposure). Alterations to the spatial distribution of emissions can have a more disproportionate influence. The ability of fate and transport models to represent such a change depends on the magnitude of northward shift considered compared to the spatial resolution of the model. For example, models such as GloboPOP[5] and BETR-Global[70] which have latitudinal resolution of ≥ 15° are not ideal if the shift is only 1–5° (i.e. total emission levels likely to remain the same in all model zones) Fate models at high spatial resolution are capable of simulating such changes but are not practical as a preliminary screening tool (e.g. for assessing large numbers of chemicals).

A preliminary calculation can be made using the Characteristic Travel Distance (CTD)[71,72]. CTD is a model-derived estimate which represents the distance travelled from a source region at which the concentration in the moving medium (i.e. air, water) is reduced to 37% (1/e) of the original value considering all fate processes (e.g. degradation, deposition). CTD can be used to calculate the concentration in the moving medium at any distance (*D*) using the following expression:

$$C_{AIR}(D) = C_{AIR}(o) \cdot (e^{(D/CTD)})^{-1}$$

In the context of CTD calculations for atmospheric transport to the Arctic, a latitudinal shift north of 1° could be assumed as a first approximation to correspond to a reduction in travel distance of approximately 110 km (a more sophisticated approach would be to estimate back-trajectories from different locations to the receptor regions of interest). The effect of this shift in emissions can then be estimated by comparing the air concentration in the Arctic based on an arbitrary distance from source (*D*, km) and the air concentration in the Arctic calculated assuming a reduced travel distance (i.e. $D - 110 \cdot n$ km, where *n* is the number of °N shifted), i.e.

$$Ratio = \frac{C_{AIR,D}(D-110n)}{C_{AIR,D}(D)} = \frac{e^{(D/CTD)}}{e^{([D-110n]/CTD)}}$$

Note that the calculated ratio is independent of distance (*D*) and therefore this calculation can be used regardless of the scenario considered assuming no change to CTD over this distance (i.e. the ratio corresponding to a shift from 35 °N to 72 °N = the ratio corresponding to a shift from 60 to 72 °N). Preliminary results are presented in Figure S12, which shows the ratio of air concentrations (spatial distribution shifted vs. default) as a function of CTD and °N shifted.

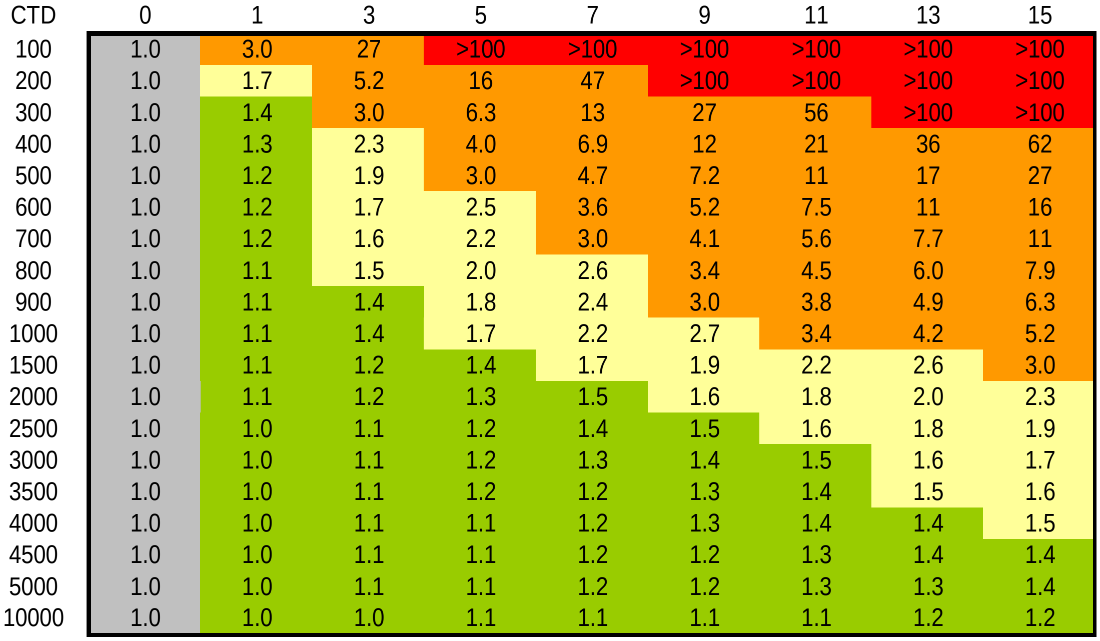

CTD	0	1	3	5	7	9	11	13	15
100	1.0	3.0	27	>100	>100	>100	>100	>100	>100
200	1.0	1.7	5.2	16	47	>100	>100	>100	>100
300	1.0	1.4	3.0	6.3	13	27	56	>100	>100
400	1.0	1.3	2.3	4.0	6.9	12	21	36	62
500	1.0	1.2	1.9	3.0	4.7	7.2	11	17	27
600	1.0	1.2	1.7	2.5	3.6	5.2	7.5	11	16
700	1.0	1.2	1.6	2.2	3.0	4.1	5.6	7.7	11
800	1.0	1.1	1.5	2.0	2.6	3.4	4.5	6.0	7.9
900	1.0	1.1	1.4	1.8	2.4	3.0	3.8	4.9	6.3
1000	1.0	1.1	1.4	1.7	2.2	2.7	3.4	4.2	5.2
1500	1.0	1.1	1.2	1.4	1.7	1.9	2.2	2.6	3.0
2000	1.0	1.1	1.2	1.3	1.5	1.6	1.8	2.0	2.3
2500	1.0	1.0	1.1	1.2	1.4	1.5	1.6	1.8	1.9
3000	1.0	1.0	1.1	1.2	1.3	1.4	1.5	1.6	1.7
3500	1.0	1.0	1.1	1.2	1.2	1.3	1.4	1.5	1.6
4000	1.0	1.0	1.1	1.1	1.2	1.3	1.4	1.4	1.5
4500	1.0	1.0	1.1	1.1	1.2	1.2	1.3	1.4	1.4
5000	1.0	1.0	1.1	1.1	1.2	1.2	1.3	1.3	1.4
10000	1.0	1.0	1.0	1.1	1.1	1.1	1.1	1.2	1.2

Figure S12 Ratio of air concentration in remote region with reduced travel distance to air concentration in remote region with default travel distance as a function of CTD (km) and number of °N shifted (*n* = 0 to 15°)

In reality, environmental conditions determining CTD change over these latitudes. However, the corresponding change in CTD could possibly be taken into account by modifying the parameterization of the model. In addition, due to atmospheric circulation patterns, shifts of emissions northwards are not as simply related to transport distance as assumed here. The travel distance from any given source location (e.g. lat, long) and a more northerly site (lat + x, long + y) could be determined more precisely (e.g. back trajectory analyses) and used in such a calculation. Note that similar approaches could be adopted for riverine and oceanic transport, at least as a first-approximation.

Section S13 Biomagnification potential and other considerations related to food-web interactions

Modelled and observed BMF_{MAX}[73] for important feeding relationships in the Arctic are presented in Table S16. With respect to model performance, 85% of the model-calculated geometric mean BMF_{MAX} values were within a factor of 2 of the available observed values. Data characterizing net growth efficiency were unavailable for many fish species, limiting the model evaluation in many cases. Marine fish exhibited relatively low observed BMF_{MAX} values, possibly due to the availability of a wide range of energetically favorable prey items. Observed BMF_{MAX} values for freshwater fish are more variable.

Table S16 Modeled and observed geometric mean BMF_{MAX} (fugacity-based ratios; comparable to BMFs expressed on a lipid-normalized basis)[73].

Consumer	Diet	Modeled BMF_{MAX} (95% CI)	Observed BMF_{MAX}* (95% CI)
Freshwater mysid (*Mysis relicta*)	zooplankton	2.7 (0.7–11)	1.9 (1–3.6)
Chaetognath (*Euchaeta glacialis*	copepods	6.4 (4.3–9.6)	3.9 (1.1–13)
Marine mysid (*Themisto libellula*	copepods	5.0 (2.9–8.5)	7.1 (1.7–30)
Polar cod (*Boreogadus saida*)	crustacean, zooplankton	1.5 (0.8–2.9)	2.5 (1.6–3.8)
Arctic cisco (*Coregonus autamnalis*)	crustacean, zooplankton	15.5 (8.6–28)	16.3 (8.1–33)
Ringed Seal, adult	cod	24.2 (15–39)	13.2 (2.8–62)
Ringed Seal, juv. (*Phoca hispida*)	fish	12.9 (7.1–23)	17.7 (7.4–42)
Walrus, male (*Odobenus rosmaris*)	mussels	14.1 (7.4–27)	17.5 (7.6–40)
Bowhead whale (*Balaena mysticetus*	copepods	22.1 (12–40)	14.7 (7.7–28)
Glaucous gull (*Larus hyperboreus*	cod	40.8 (16–106)	53.9 (20–145)
Black guillemot (*Cepphus grille*)	cod	40.1 (15–104)	18.0 (3.8–86)
Polar bear (*Ursus maritimus*)	ringed seal	57.3 (30–109)	34.7 (8.0–150)
Caribou (*Rangifer tarandus*)	lichen	11.0 (6.1–20)	12.3 (7.2–21)
Wolf, > 2 year	caribou	73.1 (20–255)	78.6 (19–330)

As discussed in the main text, BMF_{MAX} represents the maximum biomagnification factor possible assuming negligible metabolism and elimination via respiratory exchange. The relative importance of elimination via respiratory exchange compared to fecal elimination varies as a function of hydrophobicity[36]; for chemicals with relatively low log K_{OW}, exchange across the gills is the most important elimination (and uptake) route for aquatic organisms and BMF_{MAX} will not be achieved.

The theoretical relationship between bioconcentration factor (BCF, no dietary uptake), bioaccumulation factor (BAF, all uptake routes), lipid-normalized biomagnification factors (BMF) and log K_{OW} is presented for a 1 kg fish in Figure S13. These model outputs are steady-state values and were generated using AQUAWeb[74], a generic aquatic food-web bioaccumulation model. BCF and BAF are essentially equivalent for chemicals with log K_{OW}s ranging from 1–4.5; over this range of hydrophobicity, uptake and elimination via the gills are the dominant processes and hence dietary uptake has little influence on model output. BAF exceeds BCF for chemicals with log K_{OW} ranging from 4.5–9.0 (BMF_{MAX} occurs at log K_{OW} of ~ 7.0), as dietary uptake of contaminants elevates the concentration in the fish over what is achieved due to respiratory exchange. Lipid-normalized BMFs are greater than 1 across this range. The decline in BCF and BAF as log K_{OW} increases is caused by reduced bioavailability and growth dilution, which becomes the dominant (pseudo)-elimination route for extremely hydrophobic compounds (i.e. uptake is kinetically-limited). Uncertainty in the model is elevated for high log K_{OW} (> ~ 7.5) chemicals and there is also a lack of reliable empirical data available for model evaluation of such chemicals.

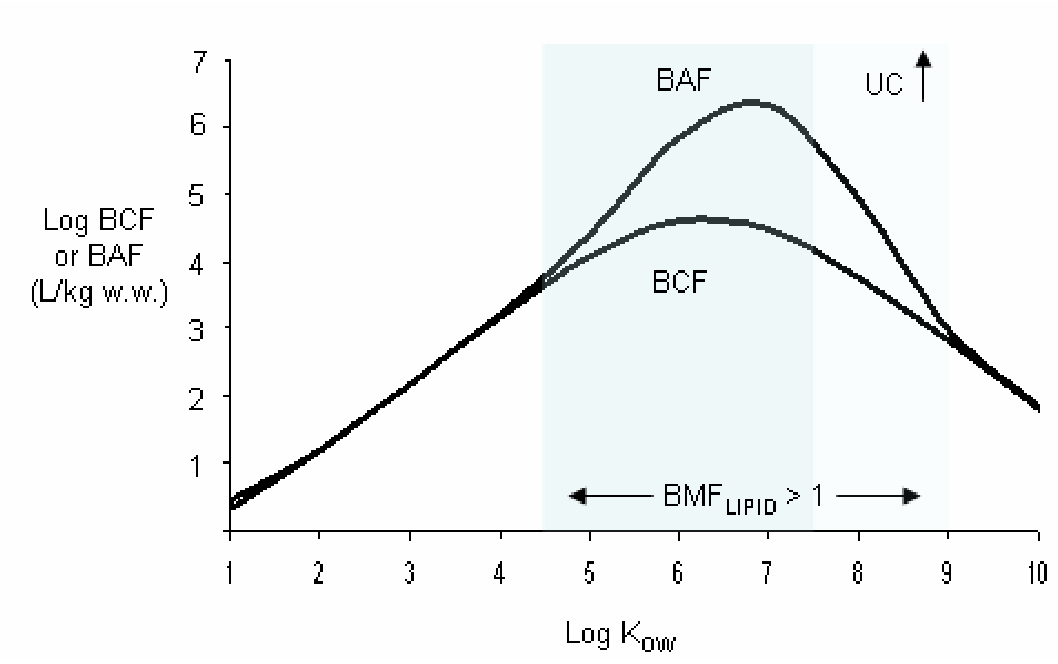

Figure S13 Steady-state BCF and BAF (L/kg w.w) vs log K_{OW} for a 1 kg piscivorous fish (pelagic, tertiary consumer, 13% lipid) as estimated by Aquaweb[74] assuming ambient water temperature of 3 °C, POC = 0.5 mg/L, DOC = 5.0 mg/L and zero biotransformation. UC = model uncertainty

Steady-state BAFs for the representative phytoplankton and zooplankton in AQUAWeb are shown in Figure S14 along with lipid-normalized BMF for zooplankton.

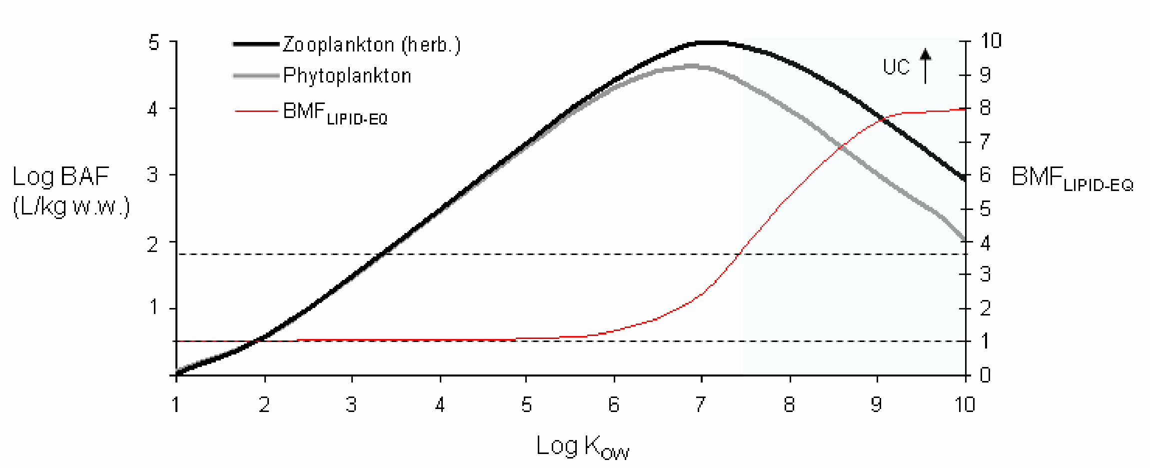

Figure S14 Steady-state lipid-normalized biomagnification factor (BMF$_{LIPID-EQ}$) for zooplankton consuming phytoplankton in comparison to log BAFs (L/kg w.w.) for zooplankton and phytoplankton as a function of log K$_{OW}$ as as estimated by AQUAWeb[74] assuming ambient water temperature of 3 °C, POC = 0.5 mg/L, DOC = 5.0 mg/L and zero biotransformation. UC = model uncertainty

In this case, the extent of biomagnification in zooplankton is suppressed and lipid-normalized BMFs are not observed until log $K_{OW} > \sim 5$. Based on this model parameterization, lipid-normalized BMFs are ≤ 2 for chemicals with log K_{OW} ranging from 1.0–7.0; BMFs increase for chemicals with log $K_{OW} > 7.0$ primarily because growth rates assumed for phytoplankton are greater than those for zooplankton. Model uncertainties for fast-growing organisms like phytoplankton and zooplankton are high. Additional empirical research is required but is challenging, particularly for very hydrophobic chemicals.

Section S14 Glacial melt in the Arctic environment

Numerous empirical studies demonstrate that remote glaciers and ice caps are reservoirs and therefore potential sources for a wide range of contaminants[26,75-78]. Macdonald et al.[26] concluded that glacial melt of the Agassiz Ice Cap in the Canadian Archipelago may be of significance for DDT (but only as a short-lived, local-scale effect) but is negligible in comparison to the reservoir and mass flows associated with surface ocean waters for HCHs, chlordane, HCB and PCBs. An important first step towards extending the analysis of the potential implications of (enhanced) glacial melt to the entire Arctic is to estimate the mass of the contaminant reservoirs. This task is facilitated by recently published data providing basic information about the current surface area, mean depth and volume of the world's glaciers[79]. Data for glaciers in the Arctic are summarized in Table S17. The overwhelming majority of surface area (85%) and volume (97%) is accounted for by the Greenland ice sheet.

Table S17 Surface area, mean depth and estimated volume of glaciers/ice caps in the Arctic.

Region	Area (x1000 km^2)	Mean Depth (m)	Est. Volume (x1000 km^3)
Greenland			
Total	1748	1677	2930
Ice sheets	1699		
Mountain glacier/ice caps	49		
Iceland	11	326	3.7
Svalbard	34	227	7.6
Russian Arctic			
Zemlya Frantsa Yosifa	14	140	1.9
Novaya Zemlya	24	470	11
Severnaya Zemlya & Ostrov Ushakova	20	340	6.6
Canadian Arctic	150	180	28
Alaska	75	275	20
TOTAL	2076		3008
Excl. Greenland	328		78

Empirical ice core/snow cap data summarized as a contaminant flux (e.g. ng m^{-2} yr^{-1}) are preferable for the purpose of estimating contaminant reservoirs[75]. The mass of contaminant in the glacier (R, kg) can be estimated as a first approximation using the accumulation flux (F, kg m^{-2} yr^{-1}), surface area (SA, m^2), and the number of years (n) represented in the depth profile, i.e.

$$R = F \cdot SA \cdot n$$

Illustrative examples for ΣPCBs and Dacthal are shown in Table S18.

Table S18 Example glacial/ice cap reservoir calculations for ΣPCBs and Dacthal using available site-specific monitoring data[75,77,78] and extrapolation to regional scale. (grey text indicates the accumulation flux is based on an extrapolation)

	Region	Area (x1000 km^2)	Accumulation Flux (ng m^{-2} yr^{-1})	Years	Mass (*t*)
ΣPCBs*	Canadian Arctic Islands	150	410 (±187)	30	1.8 (1.0–2.7)
	Greenland	1750	410 (±187)	30	22 (12–31)
	Total (incl. other regions)	2075	410 (±187)	30	26 (14–37)
Dacthal**	Svalbard	34	41 75	10 52	0.014 0.13
	Canadian Arctic Islands	150	0.4 (0.06 – 2.7)	10	<0.001
	Greenland	1750	41 0.4 75	10 10 52	0.7 0.007 6.8

* Mean value for Agassiz Ice Cap 1964/65 to 1992/93 (Canada)[75]; same value assumed for Greenland and all other regions

** Values for the Holtedahlfonna ice core (Svalbard) 1995–2005 and 1953-2005[77] and Devon Ice Cap (Canada) 2001–2005[78]

Assuming the same accumulation fluxes for the Greenland ice sheets as for the Agassiz Ice Cap (Canadian Arctic Islands), the estimated reservoir of ΣPCBs in this glacier is 12–31 *t* (includes 60 PCB congeners); extending the extrapolation to glaciers across the Arctic leads to an estimated reservoir of 14–37 *t*. This reservoir is relatively small compared to that estimated for mixed surface sediments of the pan-Arctic continental shelves (139 *t*, sum-7 PCBs)[80] but large compared to that recently estimated for the surface ocean mixed layer (0.25 t, sum-7 PCBs)[8]. A direct comparison between these reservoirs for sum-7 PCBs is not possible as congener-specific data are not reported for the Ice Cap data[75]. Somewhat surprisingly, mono and di-PCBs (PCBs 1+6+15) typically account for ≥ 50% of the reported fluxes[75]. Another major uncertainty inherent to these calculations is the extrapolation from a site-specific core to regional-scale. For example, the accumulation flux of Dacthal at a site on Svalbard is two orders of magnitude greater than at the Devon Ice Cap (Canada) for 2005 despite the relatively high atmospheric half-life (36 d) and long-range transport potential of this compound (2690 km)[77,78]. Since measured accumulation fluxes (net) represent not only gross depositional fluxes but also further processing at the site, high intra and inter-site variability may be the norm. Further empirical studies could help elucidate the extent and causes of this variability.

The mass of contaminant entering aquatic ecosystems as a result of glacial melt can be estimated from the concentration of contaminant in melt water and the volume of melt water produced annually across the Arctic. As noted elsewhere[26,81], glacial run-off is often predominantly composed of old ice (pre-industrial), mixing with which results in dilution of the contaminant load. Therefore, in the absence of measured melt water concentrations, measured concentrations in the ice core need to be adjusted to account for dilution[82,83]; the ratio of contaminated depth (i.e. depth of core) to total mean depth of glacier might be useful as a first approximation but this assumption is highly uncertain. Measured concentrations in the sampled core could be used as a worst-case/maximum impact scenario (e.g. Macdonald et al.[26]). If so, the mass of the contaminant reservoir estimated using accumulation fluxes can be used as a constraint on melt water inputs for these calculations. For example, the average ΣPCB concentration in the layers of the Agassiz ice core[75] was reported to be 3.5 ng L^{-1}. Using this concentration and a glacial melt volume of 800 km^3 since 1960 in the Canadian Arctic[26,84], the mass of ΣPCBs estimated to have entered the marine environment of the Canadian Archipelago is 2.8 *t*, in excess of the estimated mass accumulated over time using the accumulation flux (1.0–2.7 *t*).

In summary, regional-scale comparisons of reservoirs and flows are required to put the potential importance of (enhanced) glacial melt in perspective. Lack of data and/or high uncertainty in the representativeness of available measurements are major hindrances to such efforts. Given these uncertainties, there may be some cause to revisit the potential importance of glacial melt for legacy compounds, particularly PCBs, given the low concentrations and mass inventories of sum-7 PCBs in the surface mixed layer[8].

Section S15 Illustrative example of lifetime exposure to model hydrophobic contaminant (PCB-153) in relation to dietary transition/choices

Lifetime exposure was estimated following the approach described in Quinn et al.[85] whereby model output from a fate and transport model is used as input to a representative food-web bioaccumulation model including both marine and terrestrial elements depending on the population of interest. The bioaccumulation model from CoZMoMAN[86] was used as the basic framework, which was originally developed to be representative of a temperate region food web. In order to model bioaccumulation in the Arctic, the food web component was modified according to Czub et al.[87]. Zonally averaged hypothetical steady-state emissions in the Arctic and N-Temperate regions were used to calculate concentrations in the environmental compartments using the model Globo-POP[5] based on emissions 100% to the air compartment. Steady state emissions were taken to be the average of the non-steady state emissions of PCB-153 from 1930-2100[6]. Seasonality was accounted for by applying a sinusoidal cycling of the emission rate with the maxima (amplitude of 2 as a fraction of the mean annual value) occuring in August. These concentrations were provided as input files to the modified human bioaccumulation models. The environmental concentrations in the boreal and Arctic regions were considered to be at steady-state when

$$C_n - C_{n-1} < 0.001C_n$$

where C_n is the concentration in a given compartment in year *n*.

Table S19 Steady-state concentrations in air and the surface marine environment used as input to the bioaccumulation model

Region/Model Zone	Steady-state concentration (pg m^{-3})	Region/Model Zone	Steady-state concentration (pg m^{-3})
N. Temperate (i.e. Sweden)		*Arctic*	
Air (total)	0.64	Air (total)	0.32
Water, marine (total)	1210	Water, marine (total)	54.0

For the human, the dietary composition was constant over the individuals lifetime. To represent a "worst case scenario", food consumption was set equal to the maximum values that occured between 1930 and 2005. For the imported food diet (i.e. Swedish diet), this corresponds to approximately 50 g lipid per day of dairy products, 12 g lipid per day of beef, and 75 g wet weight per day of fish. The baseline Inuit diet was parameterized according to Czub et al.[87] where seal blubber is the only dietary source of contaminants considered with a daily ingestion rate (for a female Inuit) of approximately 20 g. The remaining caloric demand is assumed to come from relatively clean food sources such as berries, plants, land mammals, and birds (e.g. the modelled concentration in caribou inhabiting the N.Boreal zone using the same approach is 0.055 ng g^{-1} lipid). Lipids derived from seal blubber were then replaced entirely by fish lipids (Arctic cod) to calculate lifetime exposure for the Inuit (no seal) diet.

The cumulative lifetime exposure was calculated by summation of the body burden over the 79 year lifetime by:

$$E_{life} = \sum_{t=0}^{t=1} C_B \cdot 1.38 \times 10^{-2} + \sum_{t=1}^{t=79} C_B$$

where C_B is modelled concentration in humans based on a given diet. By using this approach, both contaminant uptake (through dietary exposure) and elimination (growth, egestion, reproduction, metabolism, etc) are considered. This approach is more representative of actual human exposure than considering only dietary intake. The concentrations in major dietary items are summarized in Table S20 and lifetime exposures for the baseline, no seal and imported food diet are shown in Figure S15.

As expected from the concentrations in dietary lipids, lifetime exposure for the baseline Inuit diet is approximately 40 times higher than the no seal diet. As shown in Table S20 and following from the ambient environment concentrations used as input (Table S19), concentrations in fish lipids from the temperate aquatic environment (i.e. Sweden) are much higher than fish in the Arctic and on the same order of magnitude as seal blubber. However, lifetime exposure for the imported food diet is still ~ 20 times lower than the baseline diet because terrestrial food-web derived lipids (i.e. dairy and beef) dominate the overall intake.

Table S20 Lipid-normalized concentrations of PCB-153 in major food items in local foods (Arctic) compared to imported foods (boreal/Sweden).

Food Item	Concentration, ng g^{-1} (lipid-normalized)	Food Item	Concentration, ng g^{-1} (lipid-normalized)
Traditional Inuit Diet		*Imported Diet (Sweden)*	
Arctic Cod		Herring	
1 year-old	6	1 year-old	95
9 year-old	10	9 year-old	160
Seal blubber		Cod	
Male, 1-year old	35	1 year-old	95
Male, 10-year old	180	9 year-old	415
Male, 20-year old	325		
		Dairy (lipids)	0.6
Female, 1-year old	35	Beef	1.8
Female, 10-year old	155		
Female, 20-year old	280		

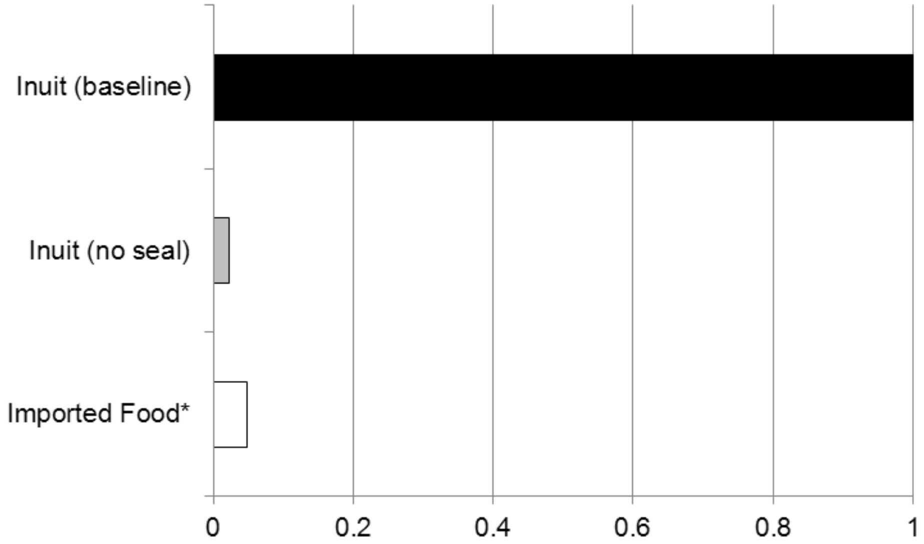

Figure S15 Lifetime exposure to PCB-153 assuming a diet high in seal blubber (baseline) relative to a diet with locally harvested fish only (no seal) and a diet representing consumption of imported food (i.e. Swedish diet)

References

1 Arctic Climate Impact Assessment (ACIA) 2005. Cambridge University Press. http://www.acia.uaf.edu.

2 D. Lavoie, K.L. Denman, R.W. Macdonald, *J. Geophys. Res.*, 2010, **115**, C04018, doi:10.1029/2009JC005493

3 I.H. Ellingsen, P. Dalpadado, D. Slagstad, H. Loeng, *Clim. Change* 2008, **87**, 155 – 175.

4 U. Schenker, M. Macleod, M. Scheringer, K. Hungerbühler, *Environ. Sci. Technol.* 2005, **39**, 8434–8441.

5 F. Wania, D. Mackay, *Sci. Total. Environ.* 1995, **160/161**, 211–232.

6 K. Breivik, A. Sweetman, J.M. Pacyna, K.C. Jones, *Sci. Tot. Environ.* 2007, **377**, 296–307.

7 European Monitoring and Evaluation Program (EMEP). Data available at http://tarantula.nilu.no/projects/ccc/emepdata.html.

8 D. Carrizo, Ö. Gustafsson, *Environ. Sci. Technol.* 2011, doi:10.1021/es103542f.

9 S.G. Donaldson, J. Van Oostdam, C. Tikhonov, M. Feeley, B. Armstrong, P. Ayotte, O. Boucher, W. Bowers, L. Chan, F. Dallaire, R. Dallaire, É. Dewailly, J. Edwards, G.M. Egeland, J. Fontaine, C. Furgal, T. Leech, E. Loring, G. Muckle, T. Nancarrow, D. Pereg, P. Plusquellec, M. Potyrala, O. Receveur, R.G. Shearer, *Sci. Tot. Environ.* 2010, **408**, 5156–5234.

10 L. Shen, F. Wania, *J. Chem. Eng. Data* 2005, **50**, 742–768.

11 H. Xiao, N. Li, F. Wania, *J. Chem. Eng. Data* 2004, **49**, 173–185.

12 A. Wong, Y.D. Lei, M. Alaee, F. Wania, *J. Chem. Eng. Data* 2001, **46**, 239–242.

13 T. Harner, M. Shoeib, *J. Chem. Eng. Data* 2002, **47**, 228–232.

14 S.A. Tittlemier, T. Halldorson, G.A. Stern, G.T. Tomy, *Environ. Toxicol. Chem.* 2002, **21**, 1804–1810.

15 F. Wania, C.B. Dugani, *Environ. Toxicol. Chem.* 2003, **22**, 1252–1261.

16 C.A. Stapleton, D.R. Peterson, T.F. Parkerton, W.J. Adams, *Chemosphere* 1997, **35**, 667–749.

17 I. Cousins, D. Mackay, *Chemosphere* 2000, **41**, 1389–1399.

18 C.A. Staples, P.B. Dorn, G.M. Klecka, S.T. O'Block, L.R. Harris, *Chemosphere* 1998, **36**, 2149–2173.

19 I.T. Cousins, C.A. Staples, G.M. Klecka, D. Mackay, *Hum. Ecol. Risk. Assess.* 2002, **8**, 1107–1135.

20 D.C.G. Muir, C. Teixeira, F. Wania, *Environ. Toxicol. Chem.* 2004, **23**, 2421–2432.

21 M. Leistra, F. van den Berg, *Environ. Sci. Technol.* 2007, **41**, 2243–2248.

22 A. Beyer, F. Wania, T. Gouin, D. Mackay, M. Matthies, *Environ. Toxicol. Chem.* 2002, **21**, 941–953.

23 M. MacLeod, M. Scheringer, K. Hungerbühler, *Environ. Sci. Technol.* 2007, **41**, 2827–2832.

24 P.N. Anderson, R.A. Hites, *Environ. Sci. Technol.* 1996, **30**, 1756–1763.

25 W.W. Brubaker Jr., R.A. Hites, *Environ. Sci. Technol.* 1998, **32**, 766–769.

26 R.W. Macdonald, T. Harner, J. Fyfe, *Sci. Tot. Environ.* 2005, **342**, 5–86.

27 R.P. Schwarzenbach, P.M. Gschwend, D.M. Imboden. Environmental organic chemistry 2nd Ed. **2003**. John Wiley & Sons Inc., Hoboken, NJ, USA.

28 L. Duforêt-Gaurier, H. Loisel, D. Dessailly, K. Nordkvist, S. Alvain, *Deep-Sea Res. I* 2010, **57**, 351–367.

29 R. Seth, D. Mackay, J. Muncke, *Environ. Sci. Technol.* 1999, **33**, 2390–2394.

30 L.P. Burkhard, *Environ. Sci. Technol.* 2000, **34**, 4663–4668.

31 K. Borgå, T.M. Saloranta, A. Ruus, *Environ. Toxicol. Chem.* 2010, **29**, 1349–1357.

32 J. Dachs, R. Lohmann, W.A. Ockenden, L. Méjanelle, S.J. Eisenreich, K.C. Jones, *Environ. Sci. Technol.* 2002, **36**, 4229–4237.

33 W-H. Xie, W-Y. Shiu, D. Mackay, *Mar. Environ. Res.* 1997, **44**, 429–444.

34 J.Z. Setschenow, J.Z. *Z. Physik. Chem.* 1889, **4**, 117–125.

35 N. Ni, S.H. Yalkowsky, *Int. J. Pharmaceut.* 2003, **254**, 167–172.

36 D. Mackay. Multimedia environmental models. The fugacity approach 2nd Ed. **2001**. Lewis Publishers, Boca Raton, FL, USA.

37 H.P.H. Arp, K-U. Goss, *Environ. Sci. Technol.* 2009, **43**, 1923–1929.

38 L.J. Thibodeaux, D. Mackay (eds). Handbook of Chemical Mass Transport in the Environment. **2011**. CRC Press Inc., Boca Raton, FL, USA.

39 R.A. Larson, E.J. Weber. Reaction Mechanisms in Environmental Organic Chemistry. **1994**. CRC Press Inc., Boca Raton, FL, USA.

40 R. Atkinson, *Chem. Rev.* 1985, 85, 69-201.

41 R. Atkinson. *J. Phys. Chem. Ref. Data Monograph No. 1.* 1989. NY: Amer. Inst. Physics & Amer. Chem Soc.

42 E.S.C. Kwok, R. Atkinson, *Atmos. Environ.* 1995, **29**, 1685–1695.

43 K. Bahm, M.A.K. Khalil, *Chemosphere* 2004, **54**, 143–166.

44 L. Lamon, M. Dalla Valle, A. Critto, A. Marcomini, *Environ. Pollut.* 2009, **156**, 1971–1980.

45 J. Lelieveld, F.J. Dentener, W. Peters, M.C. Krol, *Atmos. Chem. Phys.* 2004, **4**, 2337–2344.

46 F. Wania, *Environ. Sci. Technol.* 2003, **37**, 1344–1351.

47 T. Meyer, F. Wania, *Atmos. Environ*. 2007, **407**, 2757–2767.

48 C.M. Roth, K-U. Goss, R.P. Schwarzenbach, *Environ. Sci. Technol.* 2004, **38**, 4078–4084.

49 K-U. Goss, R.P. Schwarzenbach, *Environ. Sci. Technol.* 1999, **33**, 3390–3393.

50 C.M. Roth, K-U. Goss, R.P. Schwarzenbach, *J. Colloid. Interfac. Sci.* 2002, **252**, 21–30.

51 Y.D. Lei, F. Wania, *Atmos. Environ.* 2004, **38**, 3557–3571.

52 S. Sharma, J.R. Brook, H. Cachier, J. Chow, A. Gaudenzi, G. Lu, *J. Geophys. Res.* 2002, **107**(D24), 4771.

53 P.A. Helm, T.F. Bidleman, *Sci. Tot. Environ.* 2005, **342**, 161–173.

54 B.J. Stocks, M.A. Fosberg, T.J. Lynham, L. Mearns, B.M. Wotton, Q. Yang, J-Z. Jin, K. Lawrence, G.R. Hartley, J.A. Mason, D.W. McKenney, *Clim. Change* 1998, **38**, 1–13.

55 M.D. Flannigan, Y. Bergeron, O. Engelmark, B.M. Wotton, *J. Vege. Sci.* 1998, **9**, 469–476.

56 M.D. Flannigan, B.J. Stocks, B.M. Wotton, *Sci. Tot. Environ.* 2000, **262**, 221–229.

57 M.D. Flannigan, K.A. Logan, B.D. Amiro, W.R. Skinner, B.J. Stocks, *Clim. Change* 2005, **72**, 1–16.

58 A.J. Soja, N.M. Tchebakova, N.H.F. French, M.D. Flannigan, H.H. Shugart, B.J. Stocks, A.I. Sukhinin, E.I. Parfenova, F.S. Chapin III, P.W. Stackhouse Jr., *Global. Planet. Change* 2007, **56**, 274–296.

59 N.J. Farrar, K.E.C. Smith, R.G.M. Lee, G.O. Thomas, A.J. Sweetman, K.C. Jones, *Environ. Sci. Technol.* 2004, **38**, 1681–1685.

60 B. Gullett, A. Touati, L. Oudejans, *Atmos. Environ.* 2008, **42**, 7997–8006.

61 B.K. Gullett, A. Touati, *Atmos. Environ.* 2003, **37**, 803–813.

62 R.G.M. Lee, P. Coleman, J.L. Jones, K.C. Jones, R. Lohmann, *Environ. Sci. Technol.* 2005, **39**, 1436–1447.

63 S. Eckhardt, K. Breivik, S. Manø, A. Stohl, *Atmos. Chem. Phys.* 2007, **7**, 4527–4536.

64 D.B. Botkin, L.G. Simpson, *Biogeochemistry* 1990, **9**, 161–174.

65 J. Fang, S. Brown, Y. Tang, G. Nabuurs, X. Wang, H. Shen, *Clim. Change* 2006, **74**, 355–368.

66 S.N. Meijer, W.A. Ockenden, A. Sweetman, K. Breivik, J.O. Grimalt, K.C. Jones, *Environ. Sci. Technol.* 2003, **37**, 667–672.

67 S.G. Conard, E.P. Davidenko. Fire in Siberian boreal forests – Implications for global climate and air quality. 1998. USDA Forest Service General Technical Report PSW-GTR-166. http://www.treesearch.fs.fed.us/pubs/26956.

68 N. Spichtinger, R. Damoah, S. Eckhardt, C. Forster, P. James, S. Beirle, T. Wagner, P.C. Novelli, A. Stohl, *Atmos. Chem. Phys. Discuss.* 2004, 2747–2779.

69 T. Primbs, A. Piekarz, G. Wilson, D. Schmedding, C. Higginbotham, J. Field, S.M. Simonich, *Environ. Sci. Technol.* 2008, **42**, 6385–6391.

70 M. MacLeod, W.J. Riley, T.E. McKone, *Environ. Sci. Technol.* 2005, **39**, 6749–6756.

71 D.H. Bennett, T.E. McKone, M. Matthies, W.E. Kastenberg, *Environ. Sci. Technol.* 1998, **32**, 4023–4030.

72 A. Beyer, D. Mackay, M. Matthies, F. Wania, E. Webster, *Environ. Sci. Technol.* 2000, **34**, 699–703.

73 A.M.H. Debruyn, F.A.P.C. Gobas, *Environ. Sci. Technol.* 2006, **40**, 1581–1587.

74 J.A. Arnot, F.A.P.C. Gobas, *Environ. Toxicol. Chem.* 2004, **23**, 2343–2355.

75 D.J. Gregor, A.J. Peters, C. Teixeira, N. Jones, C. Spencer, *Sci. Tot. Environ.* 1995, **160/161**, 117–126.

76 C.J. Young, V.I. Furdui, J. Franklin, R.M. Koerner, D.C.G. Muir, S.A. Mabury, *Environ. Sci. Technol.* 2007, **41**, 3455–3461.

77 R.M. Ruggirello, M.H. Hermanson, E. Isaksson, C. Teixeira, S. Forsström, D.C.G. Muir, V. Pohjola, R. van de Wal, H.A.J. Meijer, *J. Geophys. Res.* 2010, **115**, D18308, doi:10.1029/2010JD0I4005.

78 L. Hoferkamp, M.H. Hermanson, D.C.G. Muir, *Sci. Tot. Environ.* 2010, **408**, 2985–2994.

79 A. Ohmura, A. *Annal. Glaciol.* 2009, **50**, 144–148.

80 A. Jönsson, Ö. Gustafsson, J. Axelman, H. Sundberg, *Environ. Sci. Technol.*, 2003, **37**, 245–255.

81 H.N. Geisz, R.M. Dickhut, M.A. Cochran, W.R. Fraser, H.W. Ducklow, *Environ. Sci. Technol.* 2008, **42**, 3958–3962.

82 N. van den Brink, M. Riddle, M. van den Heuvel-Greve, I. Allison, I. Snape, J.A. van Franeker, *Environ. Sci. Technol.* 2009, **43**, 3976–3977.

83 H.N. Geisz, R.M. Dickhut, M.A. Cochran, W.R. Fraser, H.W. Ducklow, *Environ. Sci. Technol.* 2009, **43**, 3974–3975.

84 M.B. Dyurgerov, M.F. Meier, *Arct. Alp. Res.* 1997, **29**, 392–402.

85 C.L. Quinn, F. Wania, G. Czub, K. Breivik, *Environ. Health Perspect.* 2010, doi:10.1289/ehp.1002415.

86 K. Breivik, G. Czub, M.S. McLachlan, F. Wania, *Environ. Intl*. 2010, **36**, 85–91.

87 G. Czub, F. Wania, M.S. McLachlan, *Environ. Sci. Technol.* **42**, 3704–3709.